Mineralogy of Bioprecipitate Evolution over Induction Times Mediated by Halophilic Bacteria under Various Mg/Ca Molar Ratios

Zuozhen Han, Dan Li, Yanyang Zhao, Jiajia Wang, Na Guo, Huaxiao Yan, Chao Han,* Qiang Li, and Maurice E. Tucker

Read Online

ACCESS | Metrics & More | Article Recommendations | Supporting Information

ABSTRACT: In microbial mineralization experiments, the induction time of mineral precipitation is ambiguous, and this may lead to difficulties in reproducing and confirming the test results. To explore the link between induction time and microbially mediated carbonate precipitation, we report here the mineralogy and morphology of carbonate precipitates induced by the halophilic *Halomonas utahensis* WMS2 bacterium in media with various Mg/Ca molar ratios over a range of induction times. The results show that the biominerals are formed in an alkaline environment affected by ammonia secreted by *H. utahensis* WMS2 bacteria. The content of dissolved inorganic carbon increased as a result of carbonic anhydrase catalyzing the hydration of carbon

dioxide to release bicarbonate and carbonate ions. The X-ray diffraction (XRD) results show that the phase of mineral precipitated gradually changes from an unstable Mg-rich calcite to metastable monohydrocalcite and then to stable hydromagnesite with an increase in the Mg^{2+} ion concentration and induction time. The scanning electron microscopy (SEM), energy-dispersive X-ray spectroscopy (EDS), and Fourier transform infrared spectroscopy (FTIR) results show that minerals mostly change from single particles/crystallites to aggregations under the action of the microorganisms at different Mg^{2+} ion concentrations and induction times. Our experiments demonstrate that the carbonate minerals produced in the presence of microbes change significantly with the induction time, in addition to the influence of the hydrochemical factors; this indicates that the induction time is significant in determining the mineralogy of biominerals.
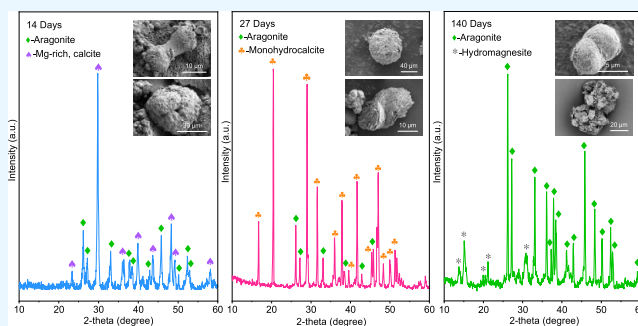
1. INTRODUCTION

In the past decades, researchers have conducted extensive research on the biomineralization of carbonate minerals, and the critical role of microorganisms in these processes has attracted much attention. Microbial mineralization is a natural process operating at the Earth's surface in many environments and even in the deep sea.[1−3] An in-depth understanding of the process of microbial mineralization is helpful to understand not only the relationship between the organic world and the inorganic world but also the formation processes of microbial rocks and to further understand the preservation mechanism of bacterial fossils.

Many researchers have conducted field investigations and simulation studies on the effect of the formation of carbonate mineral deposition mediated by microorganisms. A wealth of evidence suggests that microorganisms change the pH, alkalinity, and saturation index through their metabolic activities.[4−6] Meanwhile, during microbial-induced carbonate precipitation (MICP), organisms can generate one or more metabolic products (CO_3^{2-}) that react with cations (Ca^{2+}, Mg^{2+}) in the environment, resulting in the subsequent precipitation of minerals. In the process of biomineralization,

microorganisms not only change the surrounding microenvironment through metabolism but also provide nucleation sites through negative charges on the cell surface or within the extracellular polymeric substances (EPS) and associated viruses.[7−10]

In addition, it has been demonstrated that many factors affect the products of microbial mineralization, including temperature,[11] pressure, hydrochemical conditions,[12] organic matter,[13] and magnesium ions. Many researchers have studied the effects of Mg^{2+} ions on minerals induced by microorganisms. Magnesium ion concentration plays a very important role in regulating the type, morphology, and growth rate of minerals. Sánchez-Román et al.[14] studied the effects of 19 moderately halophilic bacteria on the precipitation of carbonate and phosphate minerals at different Mg^{2+} ion
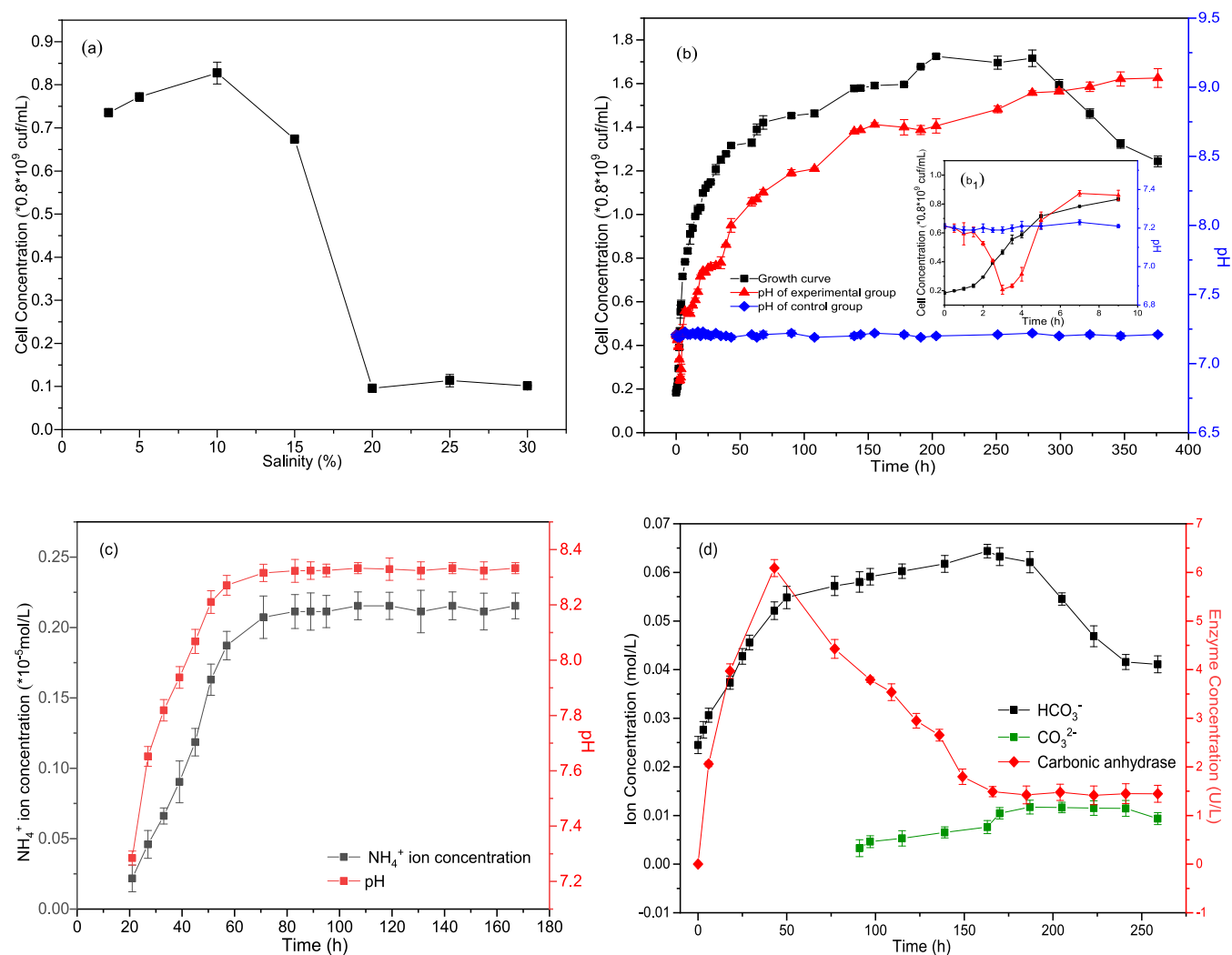
Figure 1. Basic characteristics of *H. utahensis* WMS2 bacteria. (a) Optimum salt concentration, (b) growth curve and pH value in the control group and experimental group, (c) the concentration of NH_4^+ ions and pH changes, and (d) carbonic anhydrase activity and the concentration changes of bicarbonate (HCO_3^-) and carbonate (CO_3^{2-}).

concentrations; the results showed that the percentage of Mg-rich calcite decreases and the percentage of struvite increases, and when the concentration of Mg^{2+} ion reached 0.9 M/L, only struvite ($NH_4MgPO_4 \cdot 6H_2O$) was formed. The crystalline phase produced during the conversion of amorphous calcium carbonate (ACC) depends on the concentration of the Mg^{2+} ion. High Mg calcite is precipitated in the solution with high Mg^{2+} ion concentrations and crystallized through ACC.[15] In addition, the growth rate of mineral crystals is directly proportional to the concentration of Mg^{2+} ions, that is, the higher the concentration of Mg^{2+} ions, the faster the crystal growth rate.[16]

Researchers pay more attention to a fixed time point in their experiments on microbially induced carbonate minerals, but the influence of time factors is rarely reported. Rivadeneyra et al.[17] believed that the precipitation of different kinds and contents of carbonate minerals mediated by *Nesterenkonia halobia* is affected by salinity and induction time. Sánchez-Román et al.[16] and Deng et al.[7] studied the mechanisms of carbonate mineral formation by different kinds of bacteria cultured for 30 days. *Halomonas smyrnensis* promotes the formation of carbonate minerals, with hydromagnesite formed in the presence of Mg^{2+} ions cultured for 30 days.[18] This

metastable phase is prone to degradation or transformation;[19] thus, differences in sampling times may make it difficult to compare the experimental results directly.

To clarify the influence of time factors on the precipitation of microbially induced carbonate minerals, we carried out several relevant experiments. In this study, the biomineralization selectivity of calcite, Mg-rich calcite, aragonite, monohydrocalcite (MHC), and hydromagnesite (HM) mediated by *Halomonas utahensis* WMS2 was investigated using media containing different concentrations of Mg^{2+} ions and a range of induction times. To explain the role of *H. utahensis* WMS2 in the mineral precipitation processes, growth curves, and pH curves, ammonium ion concentrations, carbonic anhydrase (CA) activity of the WMS2 bacteria in the culture medium, and the mineralogy and morphology of the precipitates formed in these groups were all carefully investigated. Herein, we show that Mg^{2+} ions and induction time can control extracellular carbonate precipitation. Under the same induction time, the mineral phases changed with the increase of Mg/Ca molar ratios. At the same time, and under the same Mg/Ca molar ratios (>2), the mineral phases also changed. In addition, intracellular carbonate minerals with lattice structures were precipitated within the halophilic bacteria themselves at a Mg/
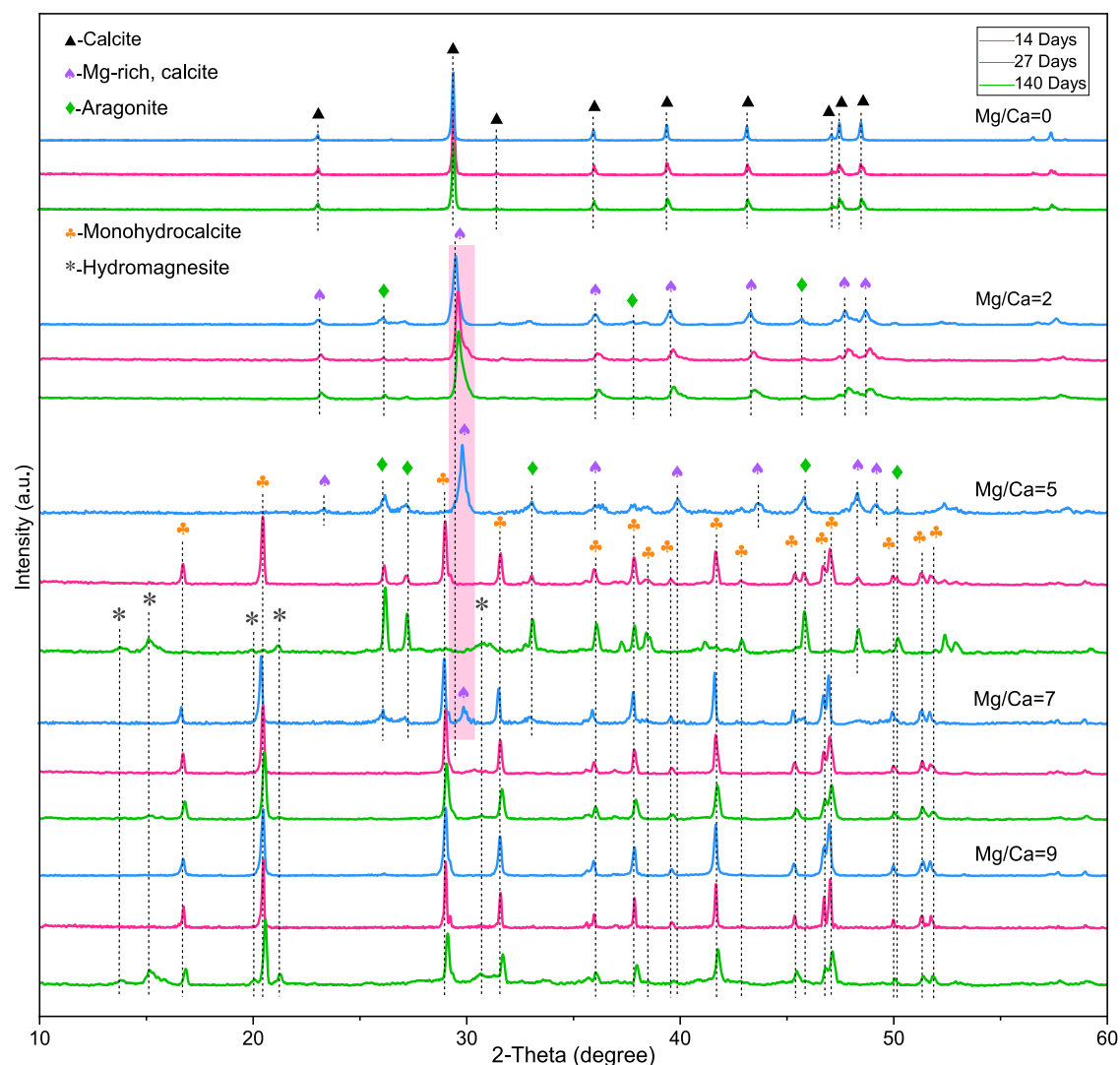
Figure 2. X-ray diffraction (XRD) analyses of the minerals induced by *H. utahensis* WMS2 bacteria at different induction times. The pink box indicates the changes in the d_{104} peak position and FWHM of the Mg-rich calcite.

Ca molar ratio of 9 cultured for 27 days. Thus, the interaction between microbial intracellular and extracellular carbonate precipitation provides a new perspective for understanding mineral formation in natural environments.

2. RESULTS

2.1. Characterization of WMS2 Bacteria. The 1477 bp fragment of the 16S rRNA gene was amplified from strain WMS2. The accession number of the strain (ON000249.1) was obtained from GenBank in which a complete 16S rRNA gene sequence was uploaded to NCBI. The phylogenetic tree of the strain was constructed by the neighbor-joining method (Figure S1). The morphology of a single cell is shown in Figure S2; the cell is rod-shaped with a length of 1.0 μm and a width of 0.5 μm. Seven elements were detected by mapping, including C, O, N, P, and Ca, as well as a small amount of S and Mg (Figure S2c−k). Gram staining of WMS2 bacteria was negative (Figure S3a). According to these results, the strain WMS2 identified is *H. utahensis*.

Through their metabolic activities, WMS2 bacteria release ammonia, as shown by the positive color reaction of the qualitative ammonia test that the color of the experimental group with bacteria changed from yellow to reddish brown compared with the control group (Figure S3b,c). The strain WMS2 can survive in media of various salinities (3, 5, 10, and 15%), and the highest OD value indicated that the optimum salinity is 10% (Figure 1a). The growth curve of WMS2 bacteria is divided into four phases, which is the same as the theoretical situation: lag phase (0−2 h), logarithmic phase (2−203 h), stationary phase (203−278 h), and decline phase (after 278 h) (Figure 1b,b$_1$). In the initial 2 h, the bacteria grew slowly, and the pH was reduced from 7.21 to 6.88, mainly due to acidification caused by the hydration of carbon dioxide produced by the bacterial degradation of organic matter.[16] In the early stage of the logarithmic growth period (3−68 h), the NH_4^+ ion concentration and pH reached their maximum values (Figure 1c). In the later stage of the logarithmic growth period (68−203 h), the concentration of NH_4^+ ions and the resulting pH remained stable. CA is present in the rising stage from 0 to 43 h and the decline stage from 43 to 166 h, and CA maintained a downward trend after 166 h (Figure 1d). In the stationary and declining stages, the concentrations of HCO_3^- and CO_3^{2-} ions are in a stable state (Figure 1d). In conclusion, with the extension of induction time, the hydrochemical compositions of the culture medium are constantly affected by

the microorganisms, and this may lead to significant changes in the minerals precipitated at different times.

2.2. Mineral Phase Analysis by XRD and FTIR. Calcium carbonate and magnesium carbonate minerals formed under the biotic systems (Figure 2 and Table 1), but interestingly, no

Table 1. Mineral Phases Mediated by *H. utahensis* WMS2 Bacteria over 14, 27, and 140 Days of Induction Times at Different Mg/Ca Molar Ratios

	induction time (days)		
Mg/Ca	14	27	140
0	calcite	calcite	calcite
2	Mg-rich, calcite; aragonite	Mg-rich, calcite; aragonite	Mg-rich, calcite; aragonite
5	Mg-rich, calcite; aragonite	aragonite; monohydrocalcite	aragonite; hydromagnesite
7	Mg-rich, calcite; aragonite; monohydrocalcite	monohydrocalcite	monohydrocalcite; hydromagnesite
9	monohydrocalcite	monohydrocalcite	monohydrocalcite; hydromagnesite

minerals were precipitated in the inorganic systems (with no microbes present) (Figure S4). The initial mineral for 14 days of bioreactors with a Mg/Ca molar ratio of 0 is calcite, and this did not change even after an induction time of 27 and 140 days. In a similar way, Mg-rich calcite and aragonite formed at a Mg/Ca molar ratio of 2 after 14, 27, and 140 days. However, the mineral phases changed significantly for the Mg/Ca molar ratio of 5. Mg-rich calcite and aragonite formed for 14 days; aragonite and MHC precipitated for the next 27 days, and aragonite and HM precipitated for 140 days. This shows that with the change of induction time, the stable aragonite is not affected by the time, whereas the unstable Mg-rich calcite is transformed into metastable MHC, and then the metastable MHC is transformed into stable HM. Moreover, for the Mg/Ca molar ratio of 7, Mg-rich calcite, aragonite, and MHC formed for 14 days and the single-phase MHC appears for 27 days. A mixture, of MHC and HM formed for 140 days. Finally, for a Mg/Ca molar ratio of 9, MHC is present spotted for 14 and 27 days; MHC and HM were formed for 140 days, similar to the result for the medium with a Mg/Ca molar ratio of 7. As can be observed, with the increase of Mg^{2+} ion concentration (≥ 7), the formation and stability of aragonite are affected. Obviously, these results demonstrate that Mg^{2+} ions and induction time have significant effects on the carbonate mineral phases under certain conditions.

In addition, the characteristic vibrational bands of the minerals at different Mg/Ca molar ratios and induction times were analyzed by FTIR (Figure S5 and Table S1). The location peaks of 2927, 2872, 2514, 1795, 872, and 712 cm^{-1} are typical calcite. The position peak of obvious Mg-rich calcite appears at 1415, 870, and 711 cm^{-1}. Aragonite was proved to have characteristic peaks of 1508, 1488, 1084, and 856 cm^{-1}. Characteristic peaks, 1484, 1067, 870, 763, and 700 cm^{-1}, prove the existence of MHC. In addition, the position peaks of 3649, 1427, 792, and 592 cm^{-1} represent HM. The results show that vibration bands of several minerals were detected, which are consistent with the results of XRD. The XRD data were processed through the Rietveld refinement (Figure S6). By calculation, for a Mg/Ca molar ratio of 2, with the extension of induction time, the content of Mg-rich calcite decreases, whereas the content of aragonite increases. This

shows that induction time is conducive to the formation of stable aragonite compared with that of the unstable Mg-rich calcite.

The interplanar spacing (d_{104}) and full width at half-maximum (FWHM) of Mg-rich calcite decrease, and 2θ is offset right (pink box in Figure 2) at Mg/Ca molar ratios of 2, 5, and 7 for 14 days (Table S2). The content of Mg in Mg-rich calcite is 2.93, 13.08, and 16.68%, respectively. Similarly, for a Mg/Ca molar ratio of 2, the d_{104} of Mg-rich calcite also decreases and 2θ is also offset right (pink box in Figure 2) at different induction times (Table S3); the content of Mg in Mg-rich calcite is 2.93, 7.07, and 8.02%, respectively. This also shows that more Mg^{2+} ions enter the Mg-rich calcite lattice with the extension of the induction times, which affects its crystallinity. Therefore, the above results indicate that the concentration of Mg^{2+} ion and induction time play vital roles in forming the crystal structure of Mg-rich calcite.

The crystallinity of MHC formed in different induction times was compared at a Mg/Ca molar ratio of 7 (Table S4). The FWHM of the (11−1), (11−2), (22−2), and (141) crystal planes increased with the increase of induction time, indicating that the degree of MHC crystallinity became weaker. The results further show that the stability of MHC is related to the induction time.

2.3. Morphological Characteristics of Carbonate Mineral Precipitates. Generally speaking, abiotic calcite is usually rhombohedral,[20] whereas biotic calcite formed at a Mg/Ca molar ratio of 0 and different induction times is more complex, including dumbbell, long rod, and irregular rhombohedral (Figure 3a$_1$−a$_4$,b$_1$,b$_2$,c$_1$,c$_2$). At the same time, mineral aggregates begin to form with the extension of the induction time (Figure 3b$_3$,b$_4$,c$_3$,c$_4$). EDS analysis of typical minerals shows that the elements mainly include Ca, C, O, and P; some minerals also contain S (Figure S7a−d). For the Mg/Ca molar ratio of 2, aragonite has a typical cruciform shape (Figure 3d$_1$,e$_1$,f$_1$); the morphology of Mg-rich calcite is varied and includes long rod (Figure 3d$_2$,f$_4$), dumbbell (Figure 3d$_3$,e$_3$,f$_2$,f$_3$), and spherical (Figure 3e$_2$) shapes. The elemental composition of minerals is analyzed by EDS, including Ca, C, O, Mg, and P (Figure S7e−i). The presence of Mg from the EDS results shows that aragonite is formed through the action of microorganisms (Figure S7f).

The morphology of minerals for a Mg/Ca molar ratio of 5 is shown in Figure 4. For 14 days, minerals with dumbbell and irregular-to-spheroidal shapes were formed (Figure 4a$_1$−a$_4$). However, with the increase in induction time (27 days), the minerals were more twisted (Figure 4b$_1$), dumbbell (Figure 4b$_2$,b$_3$), and spheroidal (Figure 4b$_5$) shaped. Interesting morphological features such as a new mineral, HM composed of honeycomb polycrystals of dumbbell type (Figure 4c$_3$,c$_8$), spheroidal (Figure 4c$_5$), and flower shape (Figure 4c$_7$) were formed in addition to the MHC of dumbbell type (Figure 4c$_1$) and spheroidal (Figure 4c$_2$) for 140 days. The EDS results of the mineral surface include Ca, C, O, and Mg, and some minerals also have P element (Figure S8a−k), while the elemental composition of the mineral surface in Figure 4b$_4$ is only Ca, C, O, and P (Figure S8e).

At a Mg/Ca molar ratio of 7, many irregular mineral aggregates began to appear for 14 days (Figure 5a$_1$,a$_3$,a$_5$), and the surface of the mineral is composed of an irregular geometry (Figure 5a$_2$,a$_4$). For 27 days, the morphologies of minerals are dumbbell (Figure 5b$_1$), twisted (Figure 5b$_2$), spherical (Figure 5b$_3$), and long rod types (Figure 5b$_5$), and there is dissolution
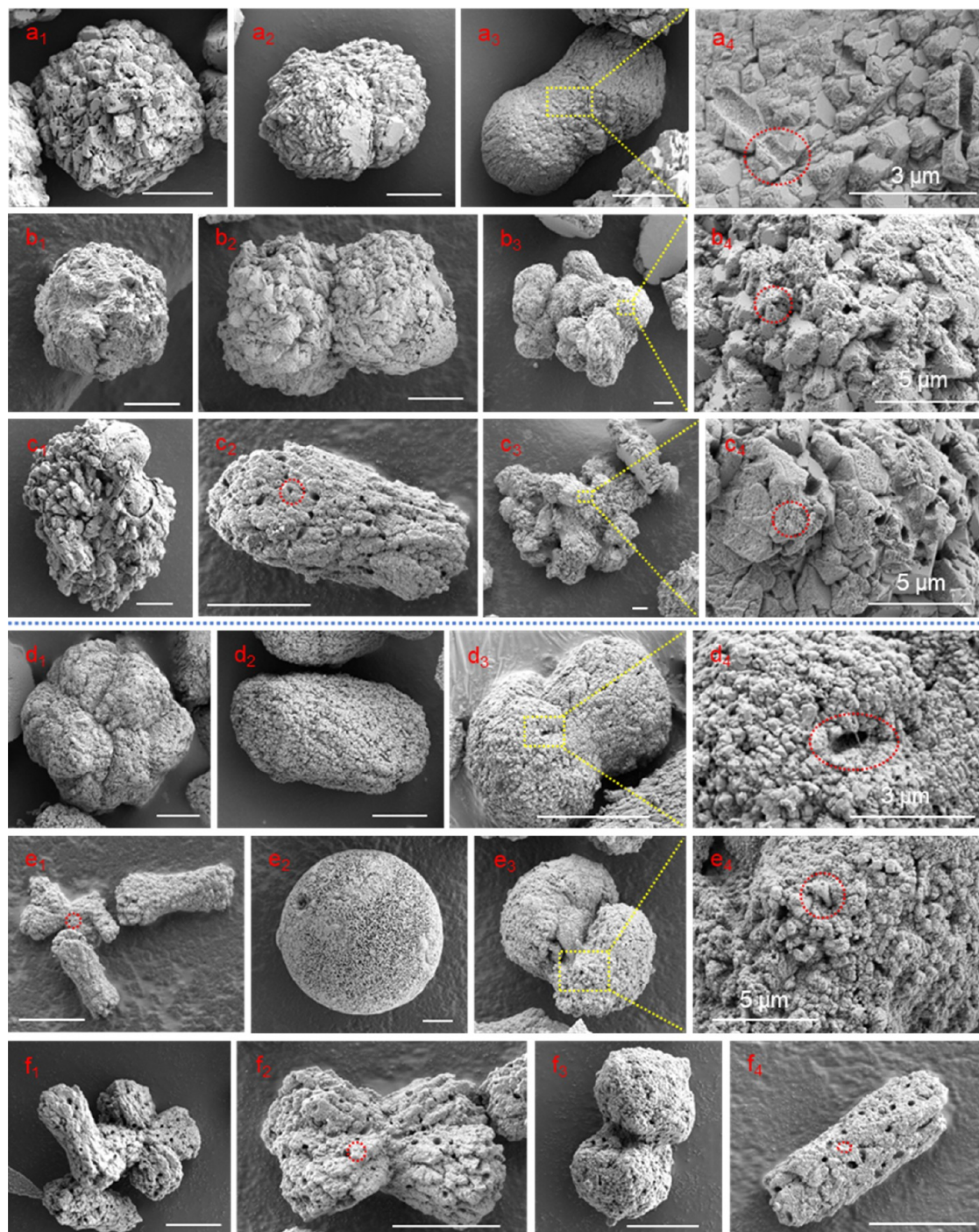
Figure 3. SEM images of microbially induced minerals at a Mg/Ca molar ratio of 0 cultured for 14 days (a_1–a_4), 27 days (b_1–b_4), and 140 days (c_1–c_4) and at a Mg/Ca molar ratio of 2 cultured for 14 days (d_1–d_4), 27 days (e_1–e_4), and 140 days (f_1–f_4). Panels a_4, b_4, c_4, d_4, and e_4 are enlarged pictures of the yellow box in panels a_3, b_3, c_3, d_3, and e_3, respectively. The position of the red circle is analyzed by EDS, as shown in Figure S7. White scale bars are 10 μm.

on the surface of minerals (Figure 5b_4). The mineral morphology of 140 days is mainly dumbbell-shaped (Figure 5c_1) composed of triangular cones (Figure 5c_2), and bacteria remain on the mineral surface (Figure 5c_2). In addition, the mineral morphology is dumbbell-shaped (Figure 5c_3) and spherical type (Figure 5c_4) composed of honeycomb polycrystals. Through EDS analysis, it is found that the element composition of the mineral in Figure 5c_2 is Ca, C, and O (Figure S9f), which can be proved to be calcium carbonate,

while the element composition of t mineral in Figure 5c_5 is Mg, C, and O (Figure S9g), which can be proved to be magnesium carbonate, which is consistent with the XRD results.

For a Mg/Ca molar ratio of 9, MHC exists in spheroidal (Figure 5d_1,e_2) and typical dumbbell (Figure 5d_3,d_4,e_1,e_4) forms for 14 and 27 days. And the incubation time has a certain influence on the morphology of minerals. For spherical minerals, the mineral surface at 14 days is composed of granular and rhombohedral crosses (Figure 5d_2), while the
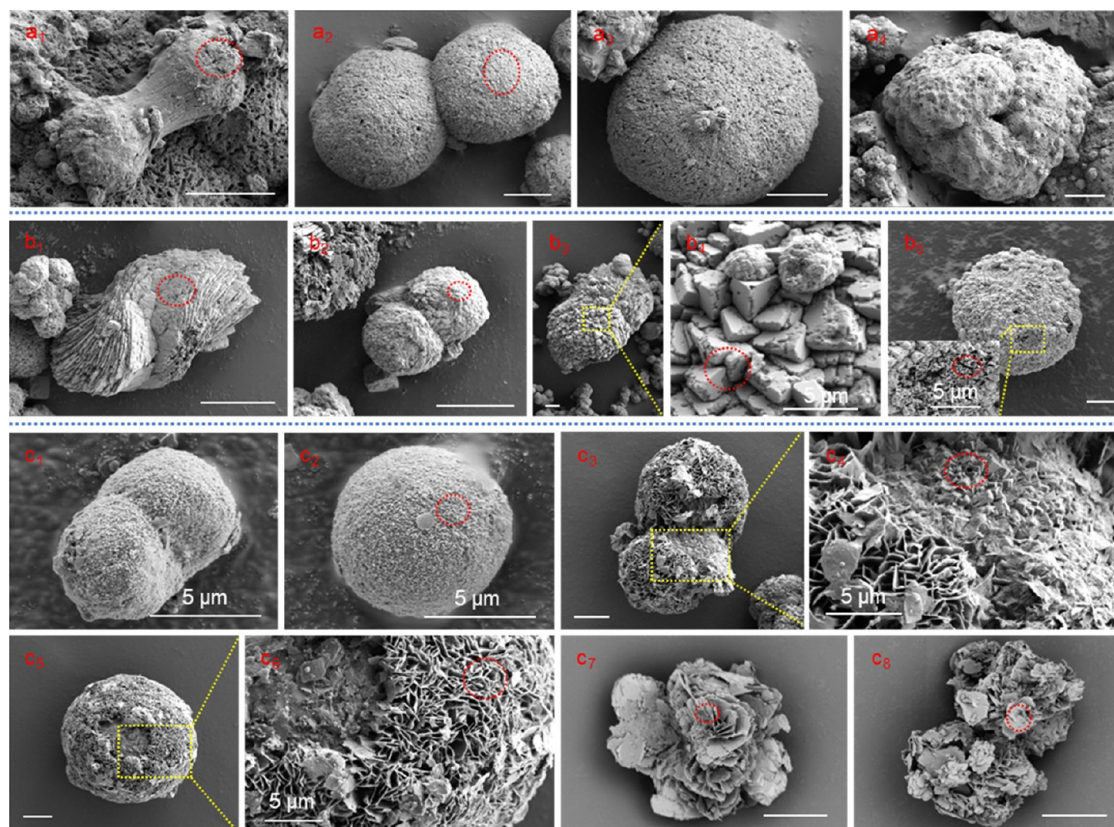
Figure 4. SEM images of microbially induced minerals at a Mg/Ca molar ratio of 5 cultured for 14 days ($a_1–a_4$), 27 days ($b_1–b_5$), and 140 days ($c_1–c_8$). Panels b_4, b_5, c_4, and c_6 are enlarged pictures of the yellow box in panels b_3, b_5, c_3, and c_5, respectively. The position of the red circle is analyzed by EDS, as shown in Figure S8. White scale bars are 10 μm.

mineral surface at 27 days is composed of triangular cones, and the phenomenon of dissolution can be seen (Figure $5e_3$). Similarly, the dumbbell-shaped mineral surface is also different. Compared with the 14 day mineral surface composed of irregular geometry (Figure $5d_3$), the 27 day mineral surface is composed of particles (Figure $5e_1$). It is worth noting that with the increase in induction time, the minerals become aggregates for 140 days, including the MHC of aggregates composed of geometric surfaces (Figure $5f_1$), a mixture phase of MHC and HM (Figure $5f_2$), and HM on a honeycomb surface (Figure $5f_4$). The elemental composition of the mineral surface can provide evidence for the determination of the mineral phase through the EDS analysis (Figure S9h–p).

The results of EDS in Figures S7–S9 show that a small amount of P derived from phospholipids, DNA, and RNA and S derived from the bacterial metabolites was detected in addition to Ca, Mg, C, and O, indicating that the bacteria play a key role in the formation and dissolution of the minerals. To sum up, the above experimental results illustrate that the higher the Mg^{2+} ion concentration and the longer the induction time, the easier it is for minerals to form aggregates, whether it is calcium carbonate or magnesium carbonate minerals; this further proves that the Mg^{2+} ion concentration and induction time play significant roles in affecting the morphology of minerals. Furthermore, the surface of the mineral shows relics of bacteria and voids left after bacteria (pink cycle in Figures S10 and S11), signifying that the bacteria are involved in the formation of the minerals.

2.4. Stable Carbon Isotope Analysis. The stable carbon isotope values of the minerals range from −16.12 to −17.63‰

at different Mg^{2+} ion concentrations (Mg/Ca molar ratios of 0, 2, 5, 7, and 9) for 14, 27, and 140 days (Table 2). The stable carbon isotope values of the organic sources (beef extract and tryptone) are −15.21 and −17.43‰; the values of Na_2CO_3 and $NaHCO_3$ artificially added to buffer the initial pH of the solution are −22.14 and −21.06‰, whereas the value of inorganic carbon dioxide in the atmosphere is −8‰.[21] The $\delta^{13}C$ values of the microbial carbonate precipitates are close to those of beef extract and tryptone, indicating that the carbonate ions in the minerals mainly come from the oxidation of organic substances in the culture medium.

2.5. Organic Functional Groups on the Bacteria, EPS Secreted by Bacteria, and Minerals Induced by Bacteria. FTIR results show that bands of many organic compounds were detected on the bacteria, EPS secreted by bacteria, and minerals induced by bacteria (Figures 6 and S12), including O−H attributed to the hydroxyl group vibrational stretching located in 3414, 2515, and 2352 cm^{-1},[22] N−H subjected to the amine group at 3200−3600 and 1450 cm^{-1},[24] the located peaks of 2925 and 2980 cm^{-1} are ascribed to the presence of saturated carbohydrates (C−H),[23] S−H assigned to protein at 2550 cm^{-1}, carboxyl C=O assigned to the peptide bond in proteins located in 1630−1639 and 1790 cm^{-1}, C−O comes from the carboxyl group at 1410 and 1115 cm^{-1}, C−O−C attributed to the ether or glycosidic group at 1068−1081 cm^{-1}, and NO_2 assigned to the nitro group at 1160 cm^{-1}. It is found that the mineral surface has the same functional groups as bacteria and EPS secreted by bacteria, which further indicates that the mineral is formed under the action of bacteria.
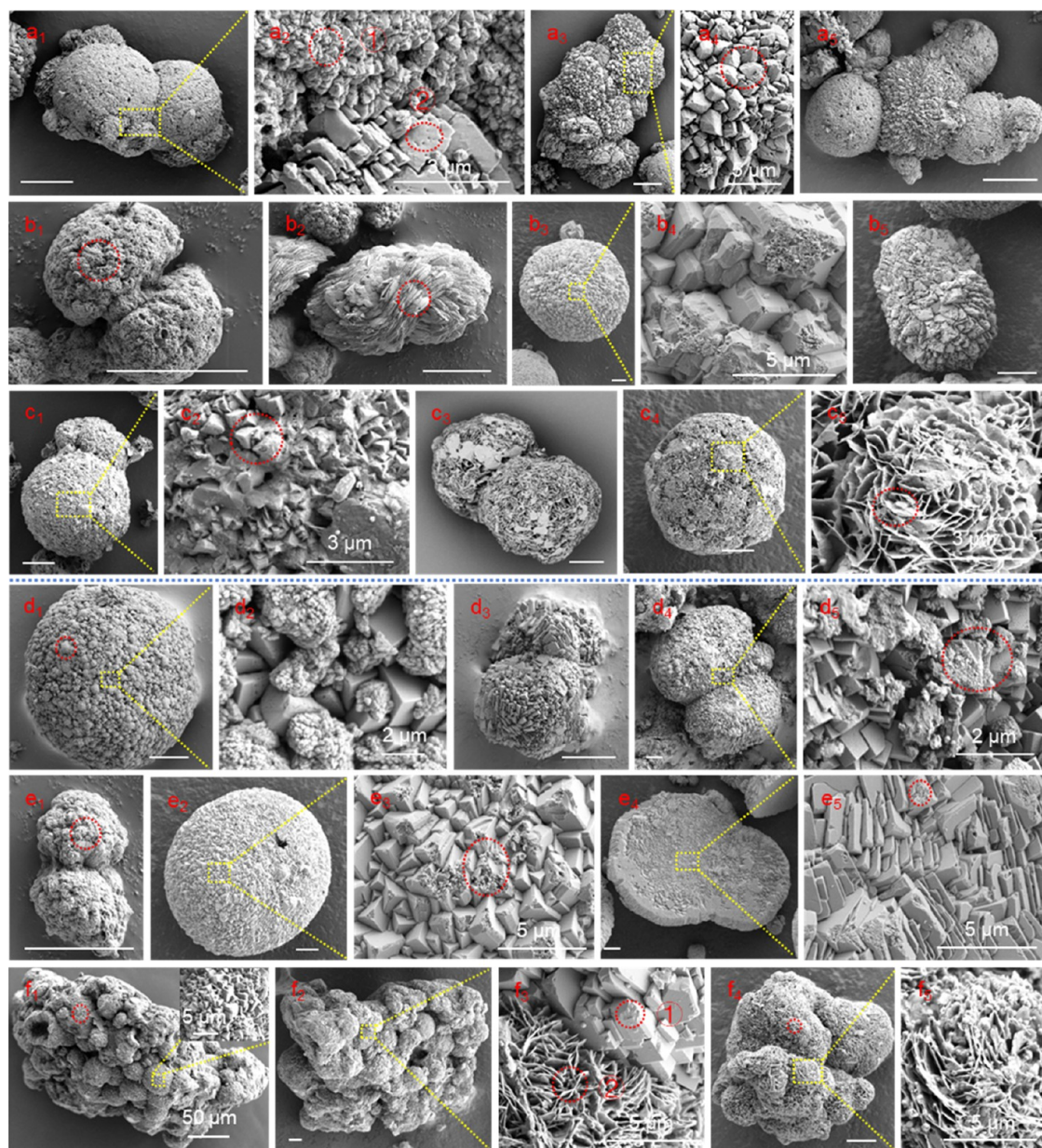
Figure 5. SEM images of microbially induced minerals at a Mg/Ca molar ratio of 7 cultured for 14 days (a_1–a_5), 27 days (b_1–b_5), and 140 days (c_1–c_5) and at a Mg/Ca molar ratio of 9 cultured for 14 days (d_1–d_5), 27 days (e_1–e_5), and 140 days (f_1–f_5). a_2, a_4, b_4, c_2, c_5, d_2, d_5, e_3, e_5, f_1, f_3, and f_5 are enlarged pictures of the yellow box in a_1, a_3, b_3, c_1, c_4, d_1, d_4, e_2, e_4, f_1, f_2, and f_4, respectively. The position of the red circle is analyzed by EDS, as shown in Figure S9. White scale bars are 10 μm.

Table 2. Stable Carbon Isotope $\delta^{13}C_{PDB}$ (‰) Values of the Minerals Induced by *H. utahensis* WMS2 Bacteria at Different Induction Times

	induction time (days)						
Mg/Ca	14	27	140	beef extract	tryptone	Na_2CO_3	$NaHCO_3$
0	−17.20	−17.39	−17.63	−15.21	−17.43	−22.14	−21.06
2	−17.32	−16.61	−16.61				
5	−16.79	−16.89	−16.95				
7	−16.21	−16.58	−16.02				
9	−16.12	−16.82	−16.28				

2.6. XPS Analysis of Mineral Surface Chemistry.

The high-resolution XPS spectrum results show that the mineral surface contains Ca, Mg, C, O, N, P, and S elements at a Mg/Ca molar ratio of 9 for 14, 27, and 140 days (Figure 7). The C

1s peak was deconvoluted into four component peaks, including the peak at 284.4 eV relating to the C−C form side chains of lipids or amino acids; the peak at 285.6 eV complies with C−OH from ether amine, alcohol, or amide
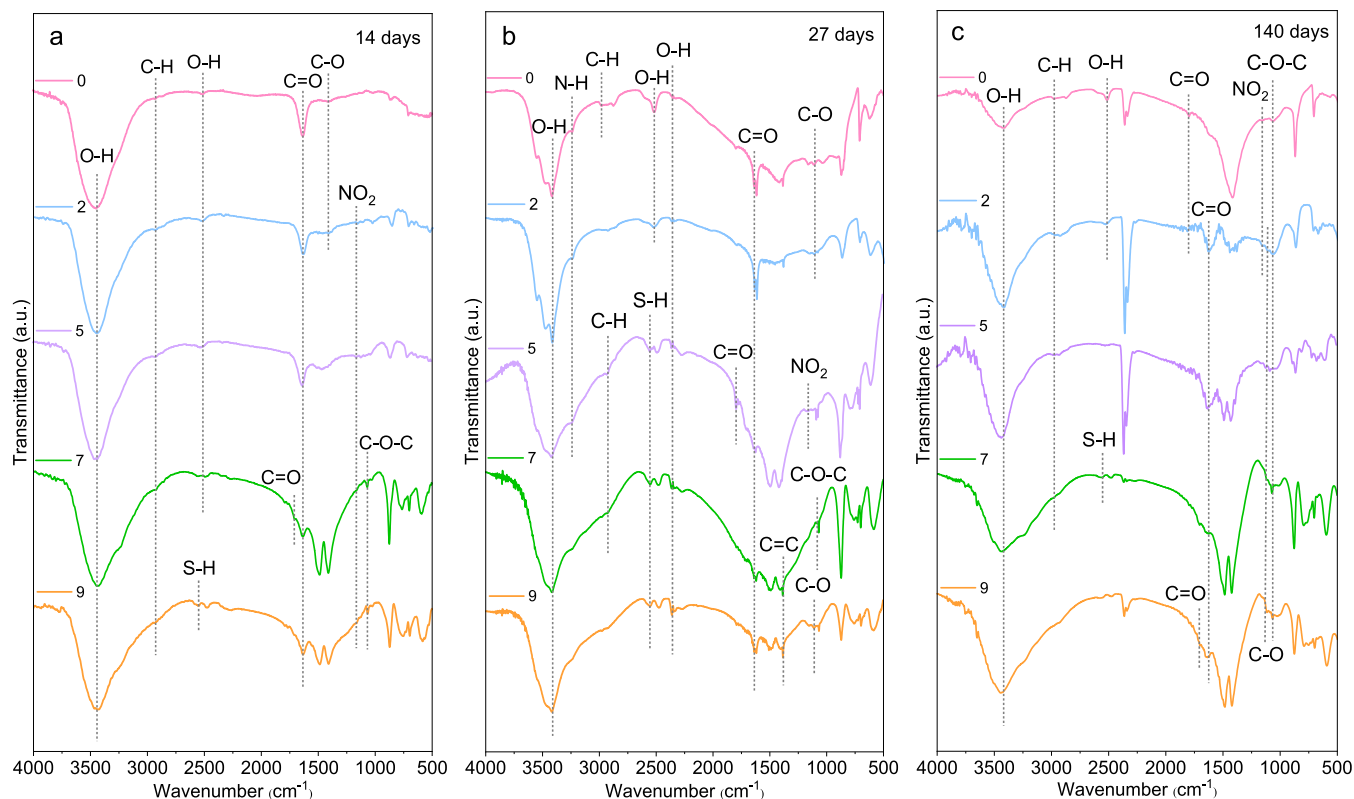
Figure 6. FTIR image of the mineral surface organic functional group at different Mg/Ca molar ratios and induction times: (a) 14 days, (b) 27 days, and (c) 140 days. 0, 2, 5, 7, and 9, respectively, represent Mg/Ca = 0, 2, 5, 7, and 9.

groups of proteins;[25,26] the peaks at 287.9, 288.2, and 288.5 eV are attributed to C═O—OH from glutamic acid and aspartic acid in EPS; the peak at 288.9 and 289.0 eV is assigned to C═O from carboxylic acid, carboxylate, carbonyl, or amide.[25,27] The binding energies of the spectral lines of Ca 2p are located at 346.6 and 350.2 eV, representing Ca $2p_{3/2}$ and Ca $2p_{1/2}$, respectively.[28,29] The binding energy position peak of the Mg atom is located at 1303.7 eV, ascribed to the Mg—O.[30] The first peak 531.0 eV of O 1s may be attributed to CO_3, another peak associated with C—O (532.2—532.8 eV). N 1s appeared at a binding energy of 399.5 and 399.7 eV (C—NH_2) and is attributable to nonprotonated nitrogen from amines and amides.[25,31] The P 2p peak can be ascribed to P—O at 132.8—133.2 eV.[32] The peak of S 2p can be ascribed to S—S at 168.4 and 164.4 eV. Through the XPS analysis, several elements on the surface of minerals constitute different organic functional groups; this is useful to further prove the important influence of organic molecules in the process of mineralization.

2.7. Thermogravimetry (TG), Derivative Thermogravimetry (DTG), and Differential Scanning Calorimetry (DSC) Analyses. The minerals induced by WMS2 bacteria were two weight loss phases in the heating processes from room temperature to 990 °C at Mg/Ca molar ratios of 5, 7, and 9 for 27 days for the TG curve (Figure 8): the first weight loss phase in the temperature range of 130—260 °C is due to the loss of structural water in MHC;[18] the second in the temperature range 620—800 °C is ascribed to the decomposition of $CaCO_3$.[18] In the second weight loss phases, the weight loss ratios are 36.79, 36.87, and 36.91% at Mg/Ca ratios of 5, 7, and 9, respectively, suggesting that MHC stability slightly decreases with increasing Mg/Ca molar ratios. There were obviously two endothermic valleys on the DTG (Figure

8b) and the same as the TG curve. The maximum weight loss rate of the temperature of the second endothermic valley was 763.4, 755.0, and 742.2 °C, respectively, indicating that the thermal stability of MHC decreases with an increasing Mg^{2+} ion concentration.

DSC results of MHC are shown in Figure 8c. In the temperature range of 620—800 °C, the bottom temperatures of MHC at Mg/Ca molar ratios of 5, 7, and 9 are 766.9, 761.9, and 745.6 °C, and enthalpy values are 449.5, 428.6, and 335.1 J/g, respectively, indicating that the thermal stability of MHC decreases with increasing Mg^{2+} ion concentrations. The stability of monohydrate calcite is affected by the concentration of the Mg^{2+} ions.

2.8. HRTEM and SAED Image Analyses of WMS2 Bacterial Cell Wall and Intracellular Minerals. Ultrathin slices of the minerals were made to analyze the intracellular mineralized lattice structure with a Mg/Ca molar ratio of 9 cultured for 27 days.

As shown in Figure 9, HRTEM and SAED observations show mineralization forms including both intracellular (Figure 9a,d) and on cell walls (Figure 9h). Intracellular inclusions have obvious lattice fringes (Figure 9b,c,e,g). The calculated interplanar spacing and crystal plane parameters are 2.521 (003), 2.582 (212), and 2.661 (220) in the microscopic image of Figure 9b; SAED patterns from these crystals clearly exhibit spots within the diffraction rings (Figure 9c); d-spacing (d, Å) and parameters of the crystallographic planes are 1.451 (115), 1.994 (410), 3.041 (300), and 3.907 (201), respectively. The weak lattice structure is displayed, and the interplanar spacings are 1.163 (036), 1.402 (23−4), and 2.105 (312) (Figure 9e). As for the cell walls, weak crystal diffraction spots were found through the interplanar spacing (d, Å) and crystal plane
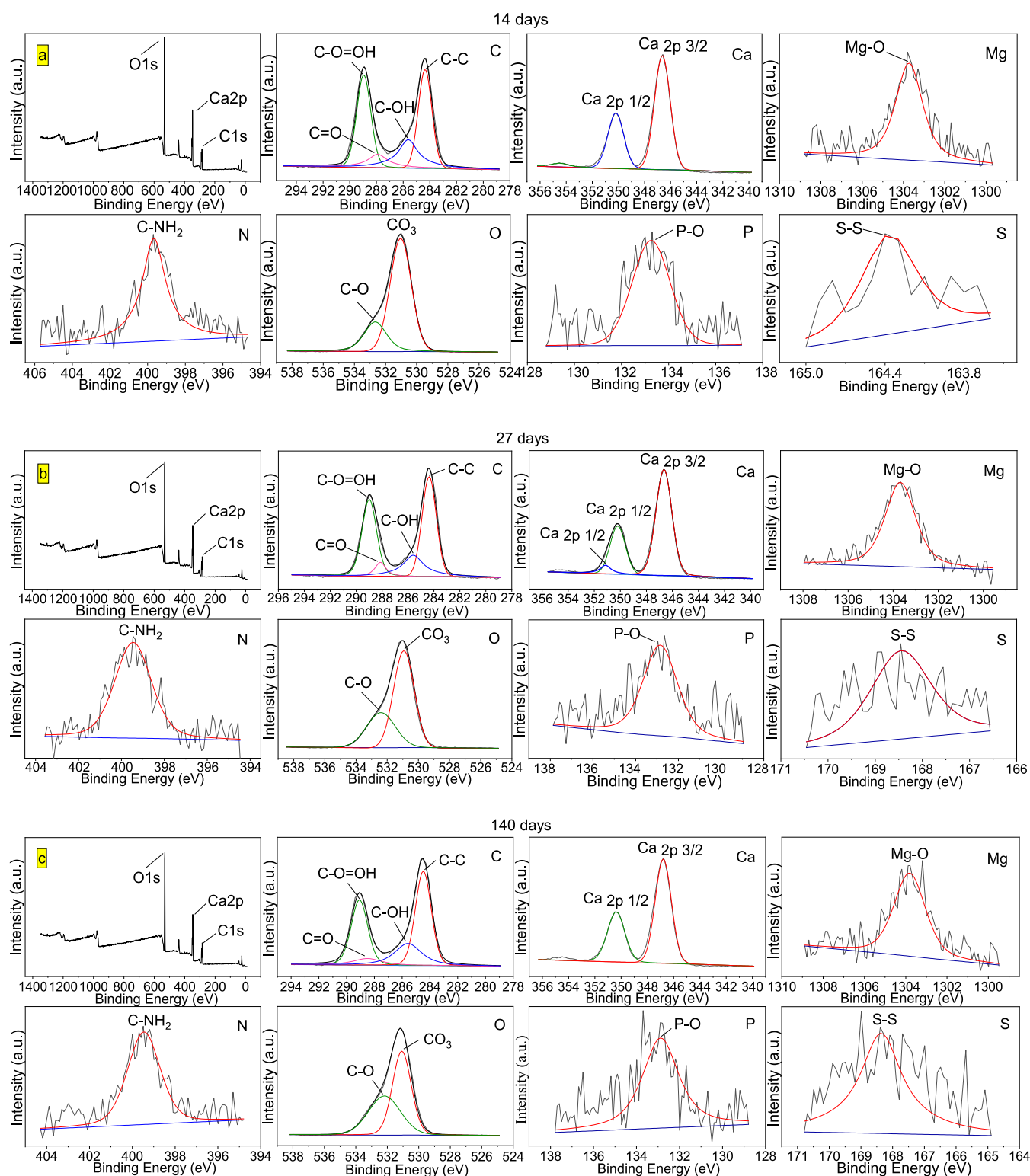
Figure 7. XPS analyses of minerals induced by *H. utahensis* WMS2 bacteria at a Mg/Ca molar ratio of 9. (a) 14 days, (b) 27 days, and (c) 140 days.

parameters are 1.843 and (104) (Figure 9g). Compared with the standard card PDF 83-1923, it can be identified as MHC inside the cell and in the cell wall. The above results are consistent with the XRD and FTIR results. Therefore, it can be inferred that the inclusions formed inside the cell are crystalline MHC through the activities of the microorganisms and presence of Mg^{2+} ions.

2.9. Amino Acid Composition of EPS from WMS2 Bacteria. Fourteen amino acids were detected from the EPS of WMS2 bacteria (Figure 10). Compared with the percentage of other amino acids, the content of Glu is the highest, up to 52.3%, and the contents of Gly and Asp acid are also high, at 8.65 and 8.33%, respectively. The acidic amino acids (AAAs) of Glu and Asp contain the carboxyl groups, demonstrating that a relatively high abundance of carboxyl groups (R—
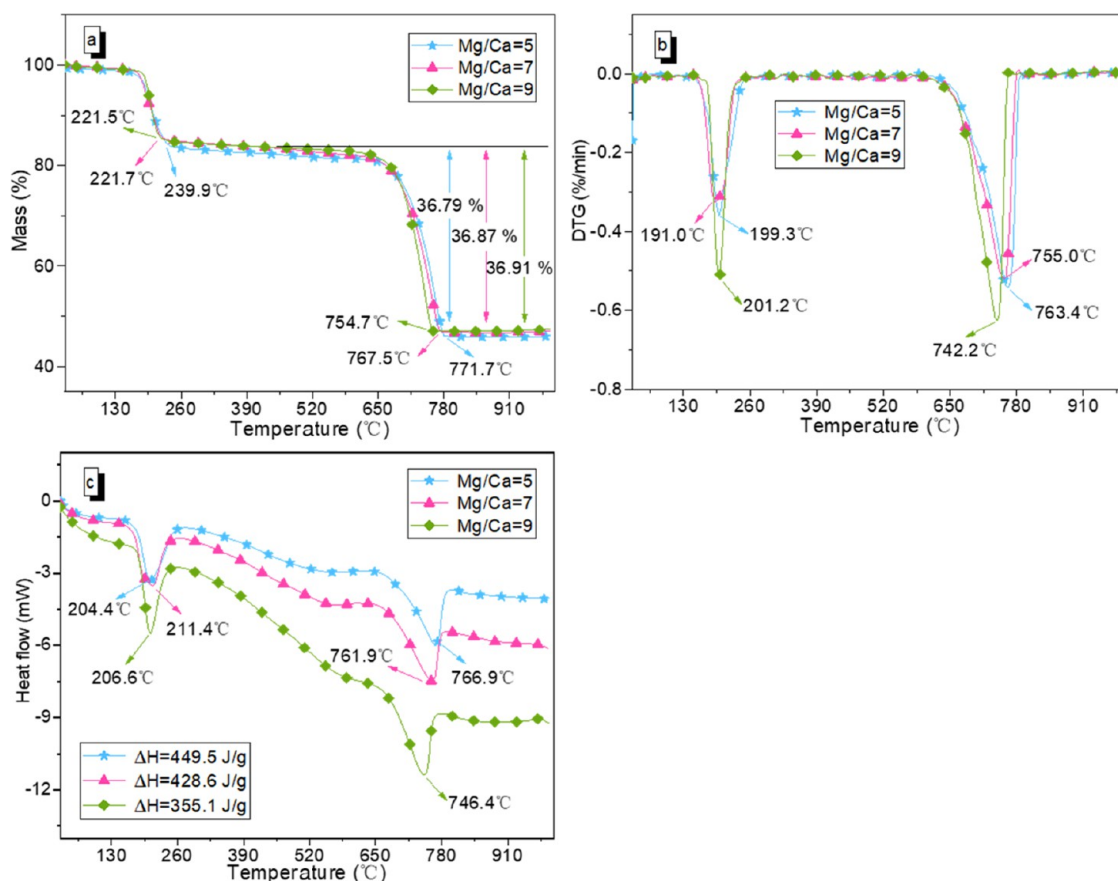
Figure 8. TG (a), DTG (b), and DSC (c) analyses of minerals induced by *H. utahensis* WMS2 bacteria at a heating rate of 20 °C/min for 27 days.

COOH) is present on bacterial cell wall surfaces. Glu and Asp acids can remove protons and become negatively charged carboxyl groups in an alkaline environment.

3. DISCUSSION

3.1. Carbon Source of Carbonate Mineral Precipitates Induced by *H. utahensis* WMS2 Bacteria. As is well known, the alkaline environment is the prerequisite for the precipitation of carbonate minerals.[33] Microorganisms can change the physical and chemical conditions of the solution through their metabolism, such as the pH value, the alkalinity of the microenvironment, and the content of dissolved inorganic carbon (DIC), which will affect the saturation of the mineral and create an environment conducive to the precipitation of carbonate minerals.[34,35] The growth of microorganisms is carried out through the use of carbon sources in the culture medium, which will lead to carbon isotope fractionation.[36] Studies have shown that the carbon and oxygen isotopes of calcium–magnesium carbonate minerals are significantly affected by the composition of environmental substances and microbial activities.[37] Microorganisms decompose organic matter to produce NH_3 and CO_2, which diffuse into pore water and significantly increase the pH, carbonate alkalinity, and saturation of the solution.[38] In this study, the tryptone and beef extract added in the experiments are degraded under the action of microorganisms; NH_3 is provided and hydrolyzed to NH_4^+ and OH^-. The NH_3 released by bacteria through the degradation of organic matter can increase the pH value of the solution and provide an alkaline environment for the formation of carbonate minerals.

In addition, bacteria produce carbon dioxide by degrading beef extract and peptone, and carbon dioxide generates bicarbonate and carbonate through hydration reactions under the catalysis of CA,[39] resulting in the increase in DIC. By comparing the measured experimental data with the carbon dioxide in the atmosphere and the reagents used in the experiment, it can be known that the carbon isotope values are closer to the values of organic substances under the action of microorganisms. The results of this study further prove that organic carbon is transferred to inorganic substances through the role of microorganisms. The combination of calcium–magnesium ions and bicarbonate or carbonate in the solution generates the magnesium carbonate minerals in an alkaline environment, realizing the storage of carbon dioxide. Therefore, it can be further confirmed that these bacteria store carbon dioxide produced by degrading organic matter in the form of carbonate precipitates.

3.2. Effect of Organic Matter on Mineral Morphology. Microbial growth and metabolism can promote mineral synthesis.[40] In previous experiments, researchers have examined the phases and morphologies of carbonate minerals formed under the action of microorganisms.[41] The microscopic appearance of minerals is diverse under the action of microorganisms and different Mg/Ca molar ratios and induction times, and their surfaces are composed of particles or geometric shapes, and many bacteria-sized pores are observed on the surface of the minerals (Figures 3–5). At the same time, it can be seen with the SEM that there are many bacteria absorbed on the surface of minerals (pink cycle in Figures S10 and S11). The primary reason is that, to adapt to
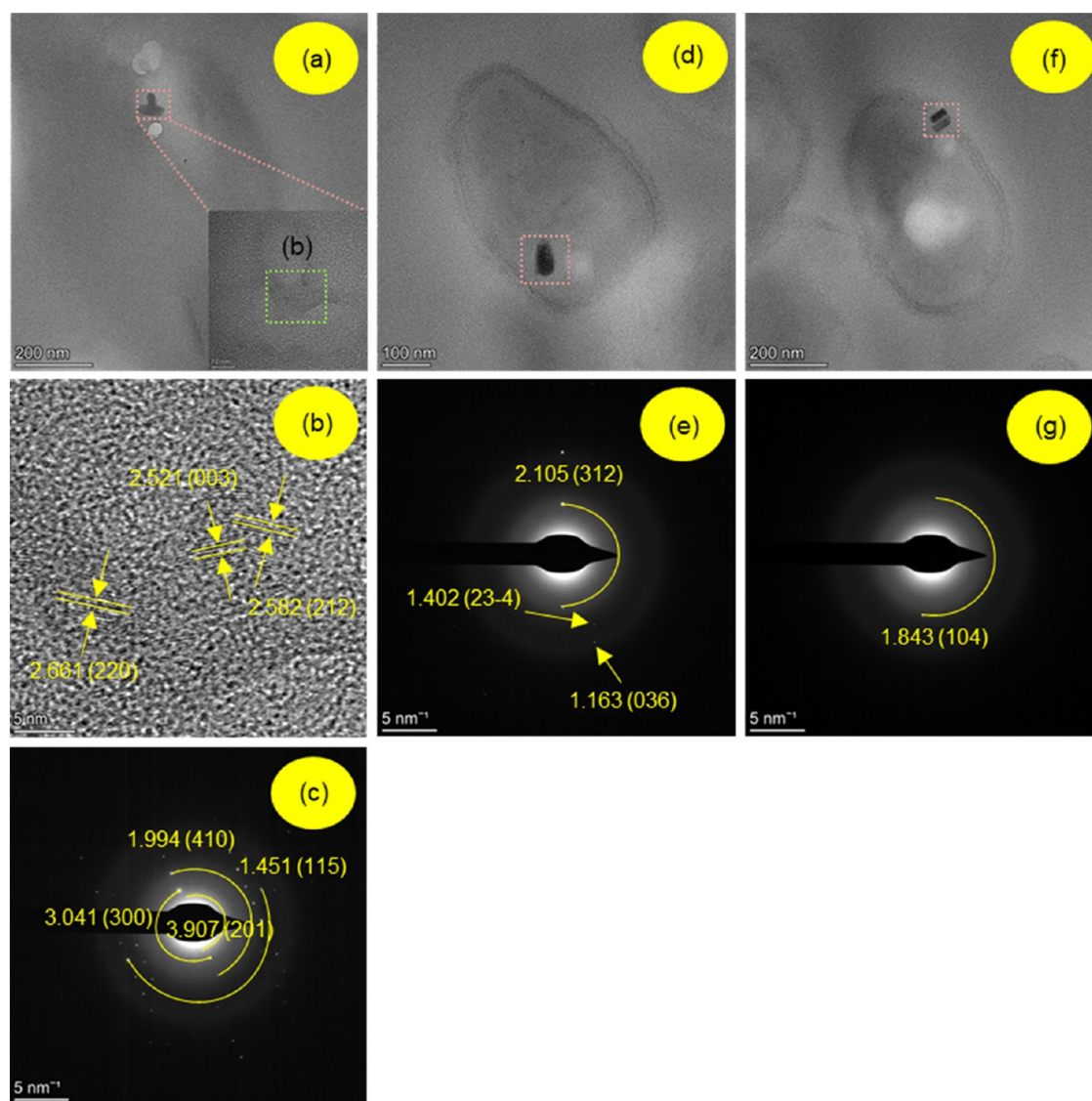
Figure 9. HRTEM and SAED images of intracellular at a Mg/Ca molar ratio of 9 culture for 27 days (Stander card: 83-1923). (a, d, f) HRTEM images of intracellular. (b) Enlarged image of the green box in panel (a). (c, e, g) SAED images of the pink box in panels (a), (d), and (f), respectively.
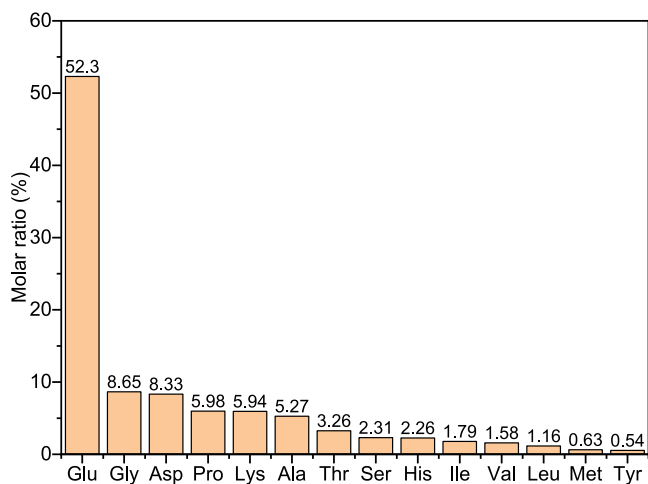

Figure 10. Amino acid composition (molar ratio) of the EPS from *H. utahensis* WMS2 bacteria.

the high ion environment, microorganisms will synthesize a large number of carboxylated molecules during the process of mineralization, which result in a variety of mineral morphology.[13]

The carboxyl group is one of the basic functional groups on the cell surface, which is generally fixed on amino acids. Glu and Asp can lose protons and become negatively charged carboxyl groups in neutral and/or alkaline environments due to the relatively low isoelectric point (average $pK_a \approx 4.7$).[42] Fourteen amino acids were detected from the EPS of WMS2 bacteria (Figure 10); among them, Glu and Asp are the two carboxyl groups that account for 60.63% of the total amino acids. In addition, the mineral surface contains C−O organic functional groups derived from the carboxyl groups, providing evidence for the existence of carboxyl groups (Figure 6). The isoelectric points of amino acids are shown in Table S5. The isoelectric points of amino acids were less than 8.0 except Lys. The role of amino acids in EPS in the process of biomineralization has two main aspects: on the one hand, WMS2 bacteria release ammonia by decomposing organic

matter and this promotes the increase of pH to above 8.0. In alkaline environments, amino acids with isoelectric points less than 8.0 are deprotonated and carry negative charges,[43,44] mainly through COO^- and $-NH^-$.[20] The deprotonated carboxyl group adsorbs Ca^{2+} and Mg^{2+} ions by electrostatic gravitation.[20] On the other hand, positively charged amino acids (Lys) can adsorb bicarbonate and carbonate anions from nearby EPS because the negatively charged carboxyl groups repel bicarbonate and carbonate in solution. Therefore, under the common effect of Lys with positive charges and amino acids with negative charges, calcium–magnesium ions and bicarbonate and carbonate ions are combined to form diverse carbonate minerals in alkaline environments.

Zhuang et al.[20] explored the biomimetic mineralization mechanism of calcium carbonate minerals using Gly (a neutral amino acid) as an organic material template through the direct precipitation method. It was found that Gly molecules can be adsorbed onto the surface of minerals or enter the interior of minerals to interact with previously formed calcite and continuously transfer electrons to dissolve calcite further. In this study, the dissolution at the surface of MHC causes corrosion and the crystallinity of the MHC decreases with the increase in Mg/Ca molar ratios cultured for 27 days (Figures 4b₁,b₅ and 5b₃,b₄,e₂−e₅). The amino acid composition of EPS of WMS2 bacteria contains a small amount of Gly (Figure 10), which may play a role in the surface dissolution of MHC.

3.3. Hydrochemical Factors Affecting Minerals.
3.3.1. Effect of Mg^{2+} Ions on Mineral Formation. Calcite is the most stable calcium carbonate mineral at room temperature and pressure; however, Mg^{2+} ions can inhibit the nucleation and formation of calcite[45−47] and can be beneficial to the formation of Mg-rich calcite, aragonite, and MHC.[48] Some Ca^{2+} ions with their larger ion radius in the calcite lattice are replaced by Mg^{2+} ions during the mineralization process since Mg^{2+} has a smaller ion radius and can enter the calcite lattice relatively easily. In addition, both hydroxyl and carboxyl groups contained within amino acids are beneficial to the dehydration of Mg^{2+}; the existence of Mg^{2+} ions is a prerequisite for the formation of these minerals (Mg-rich calcite, aragonite, and MHC). Studies have found that the presence of impurities such as Mg^{2+} ions in the growth environment of microorganisms has a very important effect on the crystal morphology.[49] Among them, Mg^{2+} ions affect the orientation of crystal growth, thereby causing lattice deformation and a change in unit cell parameters, resulting in differences in the morphology and properties of the minerals. In this experiment, with the increase of the Mg^{2+} ion concentration, the minerals change from calcite to Mg-rich calcite, aragonite, MHC, and HM, and the morphology of minerals also changes from single crystals/crystallites to aggregates. The results of this study also prove that Mg^{2+} ions have an important effect on mineral species and morphology.

Many researchers have indicated that Mg^{2+} ions are ubiquitous in the crystallization process of MHC,[50−52] and some studies have shown that a high Mg/Ca molar ratio is a prerequisite for natural and synthetic MHC.[53−55] There is no clear explanation of the formation mechanism and thermodynamic stability of MHC. Previous researchers have suggested that MHC is an unstable hydrated carbonate mineral. However, Vereshchagin et al.[52] proved that MHC is not an easily transformed intermediate phase through the results of laboratory synthesis. In this study, the crystallinity and kinetic

thermal stability of MHC at different Mg/Ca molar ratios (5, 7, and 9) were analyzed by TG-DSC. The results show that the crystallinity and thermal stability of MHC decreased as Mg/Ca molar ratios increased. It can be inferred that when the Mg/Ca molar ratio increases, more Mg^{2+} ions enter the crystal lattice and affect the crystallinity and thermal stability of MHC. Our experimental results confirm that the stability of MHC is affected by the concentration of Mg^{2+} ions to a certain extent.

3.3.2. Formation Conditions of HM. Magnesium carbonate minerals tend to precipitate in the form of various hydrated compounds at a certain temperature and solution composition.[56] More stable HM is common in natural environments; it is well known as a biological mineral precipitate in microbial mats in alkaline lakes, such as Salda Lake in Turkey, British Columbia lakes, or Alchichica Lake in Mexico.[57−59] The conditions of the formation of HM are a high pH and high Mg/Ca molar ratio.[60,61]

Previous research has shown that dolomite and magnesium carbonate are difficult to crystallize under natural and laboratory conditions, mainly because the hydration of Mg^{2+} ions reduces the presence of free Mg^{2+} ions.[62] The ion radius of the Mg^{2+} ion is small, and the charge density is high, which rationalizes the strong association between Mg^{2+} and water.[63] $[Mg(H_2O)_6]^{2+}$ is a stable inner-sphere hydration shell around the Mg^{2+} ions, which contains six water molecules in an octahedral arrangement.[64−66] In addition, it was found that the net charge on the central magnesium ion of the stable $[Mg(H_2O)_6]^{2+}$ complex was only ∼1.18,[67] indicating that significant charge transfer occurred between Mg^{2+} and the surrounding water molecules, and the covalent nature of the Mg−O bond in the hydrated shell was stronger.[63] Thereby, the process of removing water molecules around the Mg ions is the most difficult step in the formation of magnesium carbonate ($MgCO_3$) crystals. However, the water molecules in the hydrated ion of magnesium ($[Mg(H_2O)_6]^{2+}$) can be replaced by carboxyl ($RCOO^-$).[13,68] After one water molecule is replaced by carboxyl, the dehydration process of other water molecules will become easier. The free carboxyl content of Glu and Asp amino acid components in EPS derived from WMS2 bacteria increases, and this may lead to the increase of dehydrated free Mg^{2+} ions in the experimental group. After some water molecules on the hydrated ions of magnesium ($[Mg(H_2O)_6]^{2+}$) are substituted with the carboxyl group of amino acids, the dehydrated Mg^{2+} ions combine with the CO_3^{2-} ions to form magnesium carbonate minerals as follows

$$5Mg^{2+} + 4CO_3^{2-} + 2OH^- + 4H_2O$$
$$= Mg_5(CO_3)_4(OH)_2 \cdot 4H_2O\downarrow \quad (1)$$
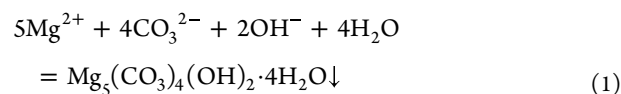
Thereby, in this study, free Mg^{2+} ions combine with carbonate to form stable HM under the action of the WMS2 bacteria.

3.4. Mineralization in the Intracellular Environment.
In recent years, intracellular mineral inclusions are present in some microorganisms, including cyanobacteria.[69−71] Ragon et al.[72] and Benzerara et al.[70] found different types of cyanobacteria that can precipitate intracellular calcium carbonate. In addition, Martignier et al.[73] reported the formation of amorphous calcium carbonate within eukaryotic cells. Yan et al.[74] found that aragonite with a crystal structure appeared in the cells of *Bacillus subtilis*, and Li et al.[75] showed MHC with the crystal structure present in the cells of *Bacillus amyloliquefaciens*. However, intracellular mineralization has rarely been found in halophilic bacteria.

Halophilic bacteria can resist the high osmotic pressure outside their cells and supplement the solute (compatible solute) through the osmotic pressure accumulated in the cell due to its unique structural characteristics and physiological properties. *Halomonas*, a typical halophilic bacterium, has a strong adaptability to temperature, salinity, and oxygen (an extremophile).[76] Calcium and magnesium ions are distributed in the cells of WMS2 bacteria (Figure S2), as shown by the experimental results of.[18] A proportion of the calcium ions are precipitated in extracellular positions, resulting in more free Mg^{2+} ions able to enter inside the cell: (1) the carboxyl group on the cell surface prevents cations from entering the cell, and this ability is greater for the larger Ca^{2+} ions than for the smaller Mg^{2+} ions; thus, Mg^{2+} ions can more easily enter the cells. (2) The ion channels of cells are selective. Ca^{2+} ions can be controlled through ion channels from extracellular to intracellular, and Mg^{2+} ions can slow down the passage of the Ca^{2+} ion by changing the activity of Ca^{2+} ion channels. Thus, the Mg^{2+} ion can enter cells by substituting the Ca^{2+} ions under the selectivity of cell ions.[12,77] (3) As a result of diffusion, the high concentration of Mg^{2+} in the solution shifts to a low concentration of cells, thus facilitating more Mg^{2+} to enter the interior of the cell. The entry of the Mg^{2+} ions into the cell provides a prerequisite for the formation of MHC.

It is well known that the production, stability, and activity of enzymes in organisms need certain physical and chemical conditions. The enzyme of halophilic bacteria is halophilic, and its production, stability, and activity need the condition of high salt concentration. The compatible solutes accumulated in cells are small, highly water-soluble molecules, such as sugar, sugar alcohol, amino acid, and its derivatives, and these can maintain low water activities in cells at a high sodium chloride concentration, so as to maintain the activity of enzymes in cells. The halophilic bacteria used in these experiments can produce CA in cells that maintain activity at a certain salt concentration; they can also be produced in cells to further catalyze carbon dioxide to synthesize carbonate and bicarbonate. In an alkaline environment and with the participation of the Mg^{2+} ions, the Ca^{2+} ions combine with carbonate or bicarbonate to form intracellular carbonate minerals. This study has shown that MHC is formed both inside and outside the cells of this halophilic bacteria and that the intracellular MHC has a crystal structure (Figure 9).

3.5. Effect of Induction Time on Minerals. Halophilic microorganisms that need a particular salinity in which to grow are very different from other microorganisms.[78] Li and Yu[79] found that *Halomonas* is the main hydrolase-producing bacteria, which is widely distributed in highly saline environments and has a unique metabolic physiological ability. Biomineralization is a complex process, which involves the physicochemical properties of the cell envelope, bacterial metabolic activities, and the characteristics of the culture medium.[80] The nature and activity of bacteria will be affected by time. With the extension of time, the amount of organic matter metabolized by WMS2 bacteria increases. When bacteria grow in the logarithmic growth phase (Figure 1b), the effect of organic matter is to increase the rate of mineral precipitation. In the later stage for WMS2 bacteria, growth is declining; bacteria growing in a highly saline environment have a unique metabolic physiological ability, leading to the production of new metabolites. The latter is conducive to the precipitation of minerals. There is no doubt that the role of

culture time in the formation of carbonate minerals cannot be ignored.

The products of mineralization in our experiments include stable calcite, aragonite, HM, unstable Mg-rich calcite, and MHC. For a Mg/Ca molar ratio of 5, the unstable Mg-rich calcite changes into metastable MHC with an extension of time. With a further increase in induction time, metastable MHC transforms into stable magnesium carbonate—HM. The mineral phases change with increasing induction time.

In previous studies, Mg-rich calcite has been synthesized using biomolecules extracted from ore-forming organisms[81] and synthetic compounds rich in carboxylic acid groups. Several studies have found that the dissolution kinetics of carbonate minerals is affected by the Mg^{2+} content,[82−84] that is, Mg^{2+} plays a key role in controlling the formation, dissolution, and diagenesis of carbonate minerals. Plummer and Mackenzie[85] demonstrated the dissolution of more soluble phases by monitoring the concentration of Mg^{2+} and Ca^{2+} ions during the dissolution of magnesium calcite. At a given carbonate ion concentration, the dissolution of the more soluble phase will lead to the dissolution being more rapid than the precipitation reaction over induction time. Blue et al.[86] and Purgstaller et al.[87] showed that under conditions of generally higher Mg/Ca molar ratios, magnesium calcite will be transformed into MHC due to the inhibition of calcite precipitation itself by the presence of Mg^{2+} ions. Crystallization time is very important for the conversion of amorphous calcium carbonate (ACC) to MHC.[52] Our experimental results verify that Mg-rich calcite dissolves first and then MHC precipitates from the effects of the Mg^{2+} ions and increased induction time.

The stability of MHC is related to the water molecules and two carbonate groups,[88] which make dehydration an energy-unfavorable process. Therefore, the conversion of inorganic MHC to other carbonates requires dissolution first, followed by precipitation. However, in the experiments with microbial participation in mineralization, biogenic MHC dose exists in the solid form in an alkaline environment due to the activities of the microorganisms. With the extension of time, some metastable MHC produced by microorganisms may spontaneously transform into more stable HM, following the thermodynamic trend. Thus, the induction time not only affects the activity of the microorganisms but it also affects the phase of carbonate minerals precipitated.

4. CONCLUSIONS

The controlling factors of mineral precipitation in microbial sediments are still controversial, mainly because of the diversity of carbonate mineral types, the microorganisms themselves, and their metabolites. To further explore the controlling factors, *H. utahensis* WMS2 bacteria, an aerobic halophilic, was used to mediate carbonate minerals under different concentrations of Mg^{2+} ions and induction times. It is found that (1) the morphology of minerals induced by WMS2 bacteria develops from a single crystallite/crystal to a variety of forms over induction time. (2) With the increase in induction time, unstable Mg-rich calcite changes to metastable MHC, which itself changes to stable HM. (3) The minerals are mainly calcium carbonate, which is due to the kinetic barrier of the hydrated Mg^{2+} ions in the initial stage of mineralization. With the consumption of Ca^{2+} ions and the secretion of a large number of organic molecules by the bacteria, the kinetic barrier of the hydrated Mg^{2+} ions is removed, more free Mg^{2+}

ions appear, and the Mg/Ca molar ratio also increases; thus, magnesium carbonate (HM) is formed with the participation of bacteria. These results show that the concentration of Mg^{2+} ions and induction time play an important role in controlling the mineralogy of carbonate minerals mediated by WMS2 bacteria and so expand our perspective on mineral precipitation through microbial processes.

5. MATERIALS AND METHODS

5.1. Enrichment and Identification of Bacteria. A large number of studies have proved that the presence of the halophilic bacteria in an evaporitic environment is closely related to the formation of various carbonate minerals; hence, halophilic bacteria were screened from a saltern and used in this research project to induce mineralization. The seed fluid medium (g/L) consisted of beef extract 5.0, tryptone 10.0, NaCl 30.0, KCl 2.0, pH 7.2. Agar of 20 g/L is added to the solid medium. 16S rDNA of the bacteria was sequenced by the Shanghai Bioengineering Co. Ltd. (Shanghai, China). The 16S rRNA sequences were submitted to GenBank to get the accession number. The phylogenetic tree was built by the neighbor-joining method. A strain named WMS2 was identified.

5.2. Basic Characteristics of WMS2 Bacteria. *5.2.1. Microscopic Morphology of WMS2 Bacteria.* The micromorphology of WMS2 bacteria was observed by high-resolution transmission electron microscopy (HRTEM, JEM-2100UHR, JEOL, Japan) by dropping the bacterial suspension onto a copper mesh and drying naturally.

5.2.2. Ammonia Test of WMS2 Bacteria. The resulting ammonia in the culture medium reacted with Nessler's reagent to produce a brown-red compound. The qualitative experiment of ammonia released from *H. utahensis* WMS2 bacteria was determined with Nessler's reagent method described by George et al.[89] and Zhuang et al.[20]

5.2.3. Determination of the Optimal Salt Concentration of WMS2 Bacteria. The optimal salt concentration for WMS2 bacteria was determined. The culture system was set up under different salt concentration conditions (NaCl: 3, 5, 10, 15, 20, 25, 30%), and each medium was inoculated with the same volume of bacterial suspension (2%) with an OD_{600} close to 1.0. The OD_{600} value of the culture medium cultured for 24 h at 37 °C and 120 rpm was measured with a spectrophotometer (722s, Shanghai Precision and Scientific Instrument Corporation, Shanghai, China).

5.2.4. Growth Curve of WMS2 Bacteria and Changes in pH of the Culture Medium. An inoculating loop was used to inoculate fresh WMS2 bacteria grown on the solid medium into the sterile liquid medium (g/L: beef extract 5.0, tryptone 10.0, NaCl 30.0, KCl 2.0, pH 7.2), after which the inoculum was incubated in an oscillation incubator (HZQ-F160, Harbin Donglian Electronic Technology Development Co., Ltd., Harbin, China) at 37 °C and 120 rpm. The concentration of the suspension was measured using spectrophotometry (722s, Shanghai Precision and Scientific Instrument Corporation, Shanghai, China) at a wavelength of 600 nm. When the OD_{600} value of the inoculum reached about 1.0, 3 mL of liquid seed was inoculated into 150 mL of sterile liquid medium and then cultured under the same conditions. At set intervals, the bacterial concentration was measured by the above method and the pH value was measured using a pH meter (PHS-3C, China).

5.2.5. Ammonium Concentration Produced by WMS2 Bacteria and pH Change Trend. To ensure the accuracy of experimental data, all glassware was carefully cleaned with a cleaning solution and then flushed out with distilled water. The cleaning solution was prepared as follows: 100 g of KOH was dissolved in 100 mL of distilled water, and 900 mL of anhydrous ethanol was added and stored in a polyethylene bottle after the solution was cooled. Ammonium concentration and pH were determined according to the detailed steps described by Zhuang et al.[20]

5.2.6. Determination of CA Activity in WMS2 Bacteria Culture Solution. To study the biomineralization mechanism of *H. utahensis* WMS2 bacteria, the CA activity of WMS2 bacteria was examined in the liquid culture medium according to the method described by Smith and Ferry.[90] One unit of CA was defined as the amount of enzyme releasing 1 μmol of *p*-nitro phenol per minute.

5.2.7. Determination of HCO_3^- and CO_3^{2-} Concentrations in WMS2 Bacterial Liquid Medium. The concentrations of HCO_3^- and CO_3^{2-} in the liquid medium were estimated by titration using the method described by Jagadeesha-Kumar et al.[91] and Zhuang et al.[20]

5.3. Mineralization Experiments. For mineralization experiments, the composition of the medium was as follows: beef extract 5.0 g/L, tryptone 10.0 g/L, NaCl 30.0 g/L, KCl 2.0 g/L, and Ca^{2+} 0.01 M. The Mg^{2+} ion concentration was 0.01, 0.02, 0.05, 0.07, and 0.09 M, respectively. Ca^{2+} and Mg^{2+} ions were provided by calcium chloride and magnesium chloride, respectively. Na_2CO_3 (21.2 g, 1 M) and 16.8 g of $NaHCO_3$ (1 M) were, respectively, dissolved in 200 mL of sterile distilled water and then filtrated by a 0.22 μm filter membrane. Three milliliters of Na_2CO_3 filtrate and 5 mL of $NaHCO_3$ filtrate were added into 150 mL of the above liquid medium at each particular Mg/Ca molar ratio. The pH was adjusted to 7.0 using NaOH and HCl solutions. The experimental group was dosed with 1% of the bacterial suspension, and the same volume of sterile water was added to the control group; each group of experiments was set with three parallel samples. The precipitates were observed with a polarized microscope every day, and the mineral component analysis was performed in continuous sampling once the mineral formation was found. The sampled interval was 14, 27, and 140 days.

5.4. Characterization of the Mineral Precipitations. Mineral precipitates were taken out from the mineralization medium under different Mg/Ca molar ratios and induction times. The mineral phases were analyzed by an X-ray powder diffraction (XRD, D/Max-RC, Rigaku, Tokyo, Japan) instrument at 40 kV and 40 mA in a 2θ angle range of $10-80$ ° with a step size of 0.02 and a count time of 8°/min. XRD data were also subjected to a Rietveld refinement analysis with the Materials Studio 7.0 program. The morphology of mineral precipitates was observed with a scanning electron microscope (SEM, Hitachi S-4800, Hitachi, Tokyo, Japan), and their elemental composition was analyzed with an energy-dispersive X-ray detector (EDX, EDAX, Mahwah, NJ) at an acceleration voltage of 20 kV and an excitation electron beam of $30-40$ μA. The phases of the mineral precipitates and organic functional groups were detected by Fourier transform infrared spectroscopy (FTIR, Nicolet 380) in the scanning range of $4000-400$ cm^{-1} with a resolution of 4 cm^{-1} by the potassium bromide tablet pressing method. The surface chemical characteristics of mineral precipitation were also analyzed by X-ray photo-

electron spectroscopy (XPS, Thermo Scientific Escalab ESCALAB 250XI, Thermo Fisher Scientific, Waltham, MA). The thermodynamic stability (TG, DTG, and DSC) of mineral precipitation for 27 days was determined by a thermogravimetric analyzer (TGA/DSC1/1600LF, Mettler Toledo Co., Schwerzenbach, Switzerland) from 30 to 1000 °C at a heating rate of 20 °C/min.

5.5. Ultrathin Slice Analysis of WMS2 Bacteria. The ultrathin slices of *H. utahensis* WMS2 bacterial cells cultivated for 27 days were prepared at a Mg/Ca molar molar ratio of 9 according to the method described by Han et al.[92] Sections (70 nm) were cut with a diamond knife on a Reichert-Jung ultracut. The distribution of intracellular elements and crystalline structures was measured using HRTEM (JEM-2011, JEOL, Japan) and SAED (Tecnai G2 F20, FEI, Hillsboro, OR).

5.6. Separation of EPS and Amino Acid Quantification. EPS of bacteria are mainly composed of polysaccharides and proteins. Amino acid, as the basic unit of protein, is also one of the components of EPS. The EPS of WMS2 bacteria were extracted with the heating method of Zhuang et al.[20] The bacterial solution in the logarithmic growth stage was collected at 2500 rpm for 8 min and washed with sterile water three times to remove impurities in the culture medium. The bacterial suspension was heated in a water bath at 60 °C for 30 min and then centrifuged at a speed of 10 000 rpm for 10 min. Finally, the transparent EPS solution was filtered by a 0.22 μm pore size filter membrane and lyophilized in a lyophilizer (FD-1A-50, Shanghai Bilang Instrument Manufacturing Co. Ltd., China) for 24 h. The EPS powder sample required to measure the amino acid content was next prepared.

The EPS powder sample (5 mg) was dissolved with 7 mL of 6 N HCl for 22 h at 110 °C in a nitrogen atmosphere and then transferred to a 10 mL volumetric flask, and after cooling, the volume was set. One milliliter of liquid from a constant volume bottle was blown at 55 °C nitrogen, and 1 mL of distilled water was added and dried, repeating three times. Twenty microliters of processed samples were tested using an amino acid analyzer (Hitachi L-8900, Tokyo, Japan), and 1.2 mL of HCl (0.02 mol/L) was added to fully dissolve, mixed well, and filtrated with a 0.45 μm membrane.

■ ASSOCIATED CONTENT

Ⓢ Supporting Information

The Supporting Information is available free of charge at https://pubs.acs.org/doi/10.1021/acsomega.2c02443.

> FTIR analysis of the characteristic peaks of minerals induced by *H. utahensis* WMS2 bacteria (Table S1 and Figure S5); characterization of minerals (Mg-rich calcite and monohydrocalcite) induced by *H. utahensis* WMS2 bacteria (Tables S2−S4); isoelectric point of amino acids from EPS of *H. utahensis* WMS2 bacteria (Table S5); phylogenetic tree, HRTEM and mapping images, and basic characteristics of *H. utahensis* WMS2 bacteria (Figures S1−S3); images of the control group during mineral experiments (Figure S4); Rietveld refinement of XRD data (Figure S6); EDS images of minerals induced by *H. utahensis* WMS2 bacteria (Figures S7−S9); SEM images of bacteria on mineral surfaces (Figures S10 and S11); and FTIR of *H. utahensis* WMS2 bacteria and EPS (Figure S12) (PDF)

■ AUTHOR INFORMATION

Corresponding Author

Chao Han − *College of Earth Science and Engineering, Shandong Provincial Key Laboratory of Depositional Mineralization and Sedimentary Minerals, Shandong University of Science and Technology, Qingdao 266590, China;* ⓘ orcid.org/0000-0002-9878-9665; Phone: (86) 0532-80681133; Email: superhan@sdust.edu.cn

Authors

Zuozhen Han − *College of Earth Science and Engineering, Shandong Provincial Key Laboratory of Depositional Mineralization and Sedimentary Minerals, Shandong University of Science and Technology, Qingdao 266590, China; Laboratory for Marine Mineral Resources, Qingdao National Laboratory for Marine Science and Technology, Qingdao 266237, China*

Dan Li − *College of Earth Science and Engineering, Shandong Provincial Key Laboratory of Depositional Mineralization and Sedimentary Minerals, Shandong University of Science and Technology, Qingdao 266590, China*

Yanyang Zhao − *College of Earth Science and Engineering, Shandong Provincial Key Laboratory of Depositional Mineralization and Sedimentary Minerals, Shandong University of Science and Technology, Qingdao 266590, China*

Jiajia Wang − *College of Earth Science and Engineering, Shandong Provincial Key Laboratory of Depositional Mineralization and Sedimentary Minerals, Shandong University of Science and Technology, Qingdao 266590, China*

Na Guo − *College of Earth Science and Engineering, Shandong Provincial Key Laboratory of Depositional Mineralization and Sedimentary Minerals, Shandong University of Science and Technology, Qingdao 266590, China*

Huaxiao Yan − *College of Chemical and Biological Engineering, Shandong University of Science and Technology, Qingdao 266590, China*

Qiang Li − *College of Earth Science and Engineering, Shandong Provincial Key Laboratory of Depositional Mineralization and Sedimentary Minerals, Shandong University of Science and Technology, Qingdao 266590, China*

Maurice E. Tucker − *School of Earth Sciences, University of Bristol, Bristol BS8 1RJ, U.K.*

Complete contact information is available at:
https://pubs.acs.org/10.1021/acsomega.2c02443

Notes

The authors declare no competing financial interest.

■ REFERENCES

(1) Holden, J.; Breier, J.; Rogers, K.; Schulte, M.; Toner, B. Biogeochemical processes at hydrothermal vents: microbes and minerals, bioenergetics, and carbon fluxes. *Oceanography* **2012**, 25, 196−208.

(2) Pisapia, C.; Gérard, E.; Gérard, M.; Lecourt, L.; Lang, S. Q.; Pelletier, B.; Payri, C. E.; Monnin, C.; Guentas, L.; Postec, A.; Quéméneur, M.; Erauso, G.; Ménez, B. Mineralizing filamentous bacteria from the prony bay hydrothermal field give new insights into the functioning of serpentinization-based subseafloor ecosystems. *Front. Microbiol.* **2017**, *8*, 57.

(3) Hu, S. Y.; Barnes, S. J.; Pagès, A.; Parr, J.; Binns, R.; Verrall, M.; Quadir, Z.; Rickard, W. D. A.; Liu, W. H.; Fougerouse, D.; Grice, K.; Schoneveld, L.; Ryan, C.; Paterson, D. Life on the edge: microbial biomineralization in an arsenic- and lead-rich deep-sea hydrothermal vent. *Chem. Geol.* **2020**, *533*, 119438.

(4) Wright, D. T.; Wacey, D. Precipitation of dolomite using sulphate-reducing bacteria from the Coorong Region, South Australia: significance and implications. *Sedimentology* **2005**, *52*, 987−1008.

(5) Rodriguez-Navarro, C.; Jimenez-Lopez, C.; Rodriguez-Navarro, A.; Gonzalez-Muñoz, M. T.; Rodriguez-Gallego, M. Bacterially mediated mineralization of vaterite. *Geochim. Cosmochim. Acta* **2007**, *71*, 1197−1213.

(6) Wang, J. J.; Zhao, Y. Y.; Li, D.; Qi, P. L.; Gao, X.; Guo, N.; Meng, R. R.; Tucker, M. E.; Yan, H. X.; Han, Z. Z. Extreme halophilic bacteria promote the surface dolomitization of calcite crystals in solutions with various magnesium concentrations. *Chem. Geol.* **2022**, *606*, 120998.

(7) Deng, S. C.; Dong, H. L.; Lv, G.; Jiang, H. C.; Yu, B. S.; Bishop, M. E. Microbial dolomite precipitation using sulfate reducing and halophilic bacteria: Results from Qinghai Lake, Tibetan Plateau, NW China. *Chem. Geol.* **2010**, *278*, 151−159.

(8) Kenward, P. A.; Goldstein, R. H.; González, L.; Roberts, J. A. Precipitation of low-temperature dolomite from an anaerobic microbial consortium: the role of methanogenic Archaea. *Geobiology* **2009**, *7*, 556−565.

(9) Tourney, J.; Ngwenya, B. T. The role of bacterial extracellular polymeric substances in geomicrobiology. *Chem. Geol.* **2014**, *386*, 115−132.

(10) Petrash, D. A.; Bialik, O. M.; Bontognali, T.; Vasconcelos, C.; Konhauser, K. O.; et al. Microbially catalyzed dolomite formation: From near-surface to burial. *Earth-Sci. Rev.* **2017**, *171*, 558−582.

(11) Al Disi, Z. A.; Zouari, N.; Dittrich, M.; Jaoua, S.; Al-Kuwari, H. A. S.; Bontognali, T. Characterization of the Extracellular Polymeric Substances (EPS) of Virgibacillus Strains capable of Mediating the Formation of High Mg-Calcite and Protodolomite. *Mar. Chem.* **2019**, *216*, 103693.

(12) Han, Y.; Sun, B.; Yan, H. X.; Tucker, M. E.; Zhao, H. Biomineralization of Carbonate Minerals Induced by The Moderate Halophile *Staphylococcus Warneri* YXY2. *Crystals* **2020**, *10*, 58.

(13) Qiu, X.; Wang, H. M.; Yao, Y. C.; Duan, Y. High salinity facilitates dolomite precipitation mediated by *Haloferax volcanii* DS52. *Earth Planet. Sci. Lett.* **2017**, *472*, 197−205.

(14) Sánchez-Román, M.; Rivadeneyra, M. A.; Vasconcelos, C.; McKenzie, J. A. Biomineralization of carbonate and phosphate by moderately halophilic bacteria. *FEMS Microbiol. Ecol.* **2007**, *61*, 273−284.

(15) Loste, E.; Wilson, R. M.; Seshadri, R.; Meldrum, F. C. The role of magnesium in stabilizing amorphous calcium carbonate and controlling calcite morphologies. *J. Cryst. Growth* **2003**, *254*, 206−218.

(16) Sánchez-Román, M.; Romanek, C. S.; Fernández-Remolar, D. C.; Sánchez-Navas, A.; McKenzie, J. A.; Pibernat, R. A.; Vasconcelos, C. Aerobic biomineralization of Mg-rich carbonates: Implications for natural environments. *Chem. Geol.* **2011**, *281*, 143−150.

(17) Rivadeneyra, M. A.; Delgado, G.; Soriano, M.; Ramos-Cormenzana, A.; Delgado, R. Precipitation of carbonates by Nesterenkonia halobia in liquid. *Chemosphere* **2000**, *41*, 617−624.

(18) Pan, J. T.; Zhao, H.; Tucker, M. E.; Zhou, J. X.; Jiang, M. Z.; Wang, Y. P.; Zhao, Y. Y.; Sun, B.; Han, Z. Z.; Yan, H. X. Biomineralization of Monohydrocalcite Induced by the Halophile *Halomonas Smyrnensis* WMS-3. *Minerals* **2019**, *9*, 632.

(19) Khanjani, M.; Westenberg, D. J.; Kumar, A.; Ma, H. Tuning Polymorphs and Morphology of Microbially Induced Calcium

Carbonate: Controlling Factors and Underlying Mechanisms. *ACS Omega* **2021**, *6*, 11988−12003.

(20) Zhuang, D. X.; Yan, H. X.; Tucker, M. E.; Zhao, H.; Han, Z. Z.; Zhao, Y. H.; Sun, B.; Li, D.; Pan, J. T.; Zhao, Y. Y.; et al. Calcite precipitation induced by *Bacillus cereus* MRR2 cultured at different Ca^{2+} concentrations: Further insights into biotic and abiotic calcite. *Chem. Geol.* **2018**, *500*, 64−87.

(21) Jones, M. B.; Donnelly, A. Carbon sequestration in temperate grassland ecosystems and the influence of management, climate and elevated CO_2. *New Phytol.* **2004**, *164*, 423−439.

(22) Karbowiak, T.; Ferret, E.; Debeaufort, F.; Voilley, A.; Cayot, P. Investigation of water transfer across thin layer biopolymer films by infrared spectroscopy. *J. Membr. Sci.* **2011**, *370*, 82−90.

(23) Dittrich, M.; Sibler, S. Calcium carbonate precipitation by cyanobacterial polysaccharides. *Geol. Soc. Lond. Spec. Publ.* **2010**, *336*, 51−63.

(24) Guo, X.; Wang, X.; Liu, J. Composition analysis of fractions of extracellular polymeric substances from an activated sludge culture and identification of dominant forces affecting microbial aggregation. *Sci. Rep.* **2016**, *6*, No. 28391.

(25) Yin, C. Q.; Meng, F. G.; Chen, G. H. Spectroscopic characterization of extracellular polymeric substances from a mixed culture dominated by ammonia-oxidizing bacteria. *Water Res.* **2015**, *68*, 740−749.

(26) Liu, R. L.; Huang, S. S.; Zhang, X. W.; Song, Y. S.; He, G. H.; Wang, Z. F.; Lian, B. Bio-mineralisation, characterization, and stability of calcium carbonate containing organic matter. *RSC Adv.* **2021**, *11*, 14415−14425.

(27) Yuan, S. J.; Sun, M.; Sheng, G. P.; Li, Y.; Li, W. W.; Yao, R. S.; Yu, H. Q. Identification of key constituents and structure of the extracellular polymeric substances excreted by *Bacillus megaterium* TF10 for their flocculation capacity. *Environ. Sci. Technol.* **2011**, *45*, 1152−1157.

(28) Bai, J.; Nagashima, T.; Yajima, T. XPS Study of apatite formed from simulated body fluid on a titanium substrate surface nitrided by an atmospheric pressure nitrogen microwave plasma. *J. Photopolym. Sci. Technol.* **2015**, *28*, 455−459.

(29) Li, H.; Yao, Q. Z.; Wang, F. P.; Huang, Y. R.; Fu, S. Q.; Zhou, G. T. Insights into the formation mechanism of vaterite mediated by a deep-sea bacterium *Shewanella piezotolerans* WP3. *Geochim. Cosmochim. Acta* **2019**, *256*, 35−48.

(30) Chen, J.; Song, Y.; Shan, D.; Han, E. H. Study of the in situ growth mechanism of Mg−Al hydrotalcite conversion film on AZ31 magnesium alloy. *Corros. Sci.* **2012**, *63*, 148−158.

(31) Dufrêne, Y. F.; Van Der Wal, A.; Norde, W.; Rouxhet, P. X-ray photoelectron spectroscopy analysis of whole cells and isolated cell walls of gram-positive bacteria: comparison with biochemical analysis. *J. Bacteriol.* **1997**, *179*, 1023−1028.

(32) Han, Z. Z.; Qi, P. L.; Zhao, Y. Y.; Guo, N.; Yan, H. X.; Tucker, M. E.; Li, D.; Wang, J. J.; Zhao, H. High Mg/Ca Molar Ratios Promote Protodolomite Precipitation Induced by the Extreme Halophilic Bacterium *Vibrio harveyi* QPL2. *Front. Microbiol.* **2022**, *13*, 821968.

(33) Lian, B.; Hu, Q.; Chen, J.; Ji, J.; Teng, H. H. Carbonate biomineralization induced by soil bacterium *Bacillus megaterium*. *Geochim. Cosmochim. Acta* **2006**, *70*, 5522−5535.

(34) Sánchez-Román, M.; Mckenzie, J. A.; Wagener, A.; Rivadeneyra, M. A.; Vasconcelos, C. Presence of sulfate does not inhibit low-temperature dolomite precipitation. *Earth Planet. Sci. Lett.* **2009**, *285*, 131−139.

(35) Diaz-Pulido, G.; Nash, M. C.; Anthony, K.; Bender, D.; Troitzsch, U.; et al. Greenhouse conditions induce mineralogical changes and dolomite accumulation in coralline algae on tropical reefs. *Nat. Commun.* **2014**, *5*, No. 3310.

(36) Lian, B.; Chen, Y.; Zhu, X.; Yang, R. Effect of microbial weathering on carbonate rocks. *Earth Sci. Front.* **2008**, *15*, 90−99.

(37) Wacey, D.; Wright, D. T.; Boyce, A. J. A stable isotope study of microbial dolomite formation in the Coorong Region, South Australia. *Chem. Geol.* **2007**, *244*, 155−174.

(38) Liu, D.; Xu, Y. Y.; Papineau, D.; Yu, N.; Fan, Q. G.; Qiu, X.; Wang, H. M. Experimental evidence for abiotic formation of low-temperature proto-dolomite facilitated by clay minerals. *Geochim. Cosmochim. Acta* **2019**, *247*, 83−95.

(39) Achal, V.; Pan, X. L. Characterization of urease and carbonic anhydrase producing bacteria and their role in calcite precipitation. *Curr. Microbiol.* **2011**, *62*, 894−902.

(40) Baskar, S.; Baskar, R.; Mauclaire, L.; McKenzie, J. A. Microbially induced calcite precipitation in culture experiments: Possible origin for stalactites in Sahastradhara caves, Dehradun, India. *Curr. Sci.* **2006**, *90*, 58−64.

(41) Bontognali, T. R. R.; Mckenzie, J. A.; Warthmann, R. J.; Vasconcelos, C. Microbially influenced formation of Mg-calcite and Ca-dolomite in the presence of exopolymeric substances produced by sulphate-reducing bacteria. *Terra Nova* **2014**, *26*, 72−77.

(42) Voegerl, R. S. Quantifying the Carboxyl Group Density of Microbial Cell Surfaces as a Function of Salinity: Insights Into Microbial Precipitation of Low-Temperature Dolomite, Thesis, University of Kansas, 2014.

(43) Dhami, N. K.; Mukherjee, A.; Reddy, M. S. Micrographical, minerological and nano-mechanical characterisation of microbial carbonates from urease and carbonic anhydrase producing bacteria. *Ecol. Eng.* **2016**, *94*, 443−454.

(44) Tanaka, M.; Mazuyama, E.; Arakaki, A.; Matsunaga, T. MMS6 protein regulates crystal morphology during nano-sized magnetite biomineralization in vivo. *J. Biol. Chem.* **2011**, *286*, 6386−6392.

(45) Bots, P.; Benning, L. G.; Rickaby, R. E. M.; Shaw, S. The role of SO₄ in the switch from calcite to aragonite seas. *Geology* **2011**, *39*, 331−334.

(46) Nielsen, M. R.; Sand, K. K.; Rodriguezblanco, J. D.; Bovet, N.; Generosi, J.; Dalby, K. N.; Stipp, S. Inhibition of calcite growth: Combined effects of Mg^{2+} and SO_4^{2-}. *Cryst. Growth Des.* **2016**, *16*, 6199−6207.

(47) Tollefsen, E.; Stockmann, G.; Skelton, A.; Mörth, C. M.; Mrth, C. M.; Dupraz, C.; Sturkell, E. Chemical controls on ikaite formation. *Mineral. Mag.* **2018**, *82*, 1119−1129.

(48) Morse, J. W. The kinetics of calcium carbonate dissolution and precipitation. *Rev. Mineral. Geochem.* **1983**, *11*, 227−264.

(49) Zhang, C. H.; Li, F. C.; Lv, J. J. Morphology and formation mechanism in precipitation of calcite induced by *Curvibacter lanceolatus* strain HJ-1. *J. Cryst. Growth* **2017**, *478*, 96−101.

(50) Nishiyama, R.; Munemoto, T.; Fukushi, K. Formation condition of monohydrocalcite from $CaCl_2$−$MgCl_2$−Na_2CO_3 solutions. *Geochim. Cosmochim. Acta* **2013**, *100*, 217−231.

(51) Rodriguez-Blanco, J. D.; Shaw, S.; Bots, P.; Roncal-Herrero, T.; Benning, L. G. The role of Mg in the crystallization of monohydrocalcite. *Geochim. Cosmochim. Acta* **2014**, *127*, 204−220.

(52) Vereshchagin, O. S.; Frank-Kamenetskaya, O. V.; Kuz'Mina, M. A.; Chernyshova, I. A.; Shilovskikh, V. V. Effect of magnesium on monohydrocalcite formation and unit cell parameters. *Am. Mineral.* **2021**, *106*, 1294−1305.

(53) Lv, D. W.; Song, Y.; Shi, L.; Wang, Z. L.; Cong, P. Z.; van Loon, A. J. The complex transgression and regression history of the northern margin of the Palaeogene Tarim Sea (NW China), and implications for potential hydrocarbon occurrences. *Mar. Pet. Geol.* **2020**, *112*, 104041.

(54) Kimura, T.; Koga, N. Monohydrocalcite in comparison with hydrated amorphous calcium carbonate: precipitation condition and thermal behavior. *Cryst. Growth Des.* **2011**, *11*, 3877−3884.

(55) Zhao, Y. Y.; Han, Z. Z.; Yan, H. X.; Zhao, H.; Tucker, M. E.; Gao, X.; Guo, N.; Meng, R. R.; Owusu, D. C. Selective adsorption of amino acids in crystals of monohydrocalcite induced by the facultative anaerobic *Enterobacter ludwigii* SYB1. *Front. Microbiol.* **2021**, *12*, 696557.

(56) Hopkinson, L.; Kristova, P.; Rutt, K.; Cressey, G. Phase transitions in the system MgO−CO_2−H_2O during CO_2 degassing of Mg-bearing solutions. *Geochim. Cosmochim. Acta* **2012**, *76*, 1−13.

(57) Russell, M. J.; Ingham, J. K. Search for signs of ancient life on Mars: expectations from hydromagnesite microbialites, Salda. *J. Geol. Soc.* **1999**, *156*, 869.

(58) Power, I. M.; Wilson, S. A.; Thom, J. M.; Dipple, G. M.; Southam, G. Biologically induced mineralization of dypingite by cyanobacteria from an alkaline wetland near Atlin, British Columbia, Canada. *Geochem. Trans.* **2007**, *8*, 13.

(59) Kamierczak, J.; Kempe, S.; Kremer, B.; López-García, P.; Moreira, D.; Tavera, R. Hydrochemistry and microbialites of the alkaline crater lake Alchichica, Mexico. *Facies* **2011**, *57*, 543−570.

(60) Berninger, U. N.; Jordan, G.; Schott, J.; Oelkers, E. H. The experimental determination of hydromagnesite precipitation rates at $22.5 - 75$ °C. *Mineral. Mag.* **2014**, *78*, 1405−1416.

(61) Gautier, Q.; Bénézeth, P.; Mavromatis, V.; Schott, J. Hydromagnesite solubility product and growth kinetics in aqueous solution from 25 to 75 °C. *Geochim. Cosmochim. Acta* **2014**, *138*, 1−20.

(62) Roberts, J. A.; Kenward, P. A.; Fowle, D. A.; Goldstein, R. H.; Gonzalez, L. A.; Moore, D. S. Surface chemistry allows for abiotic precipitation of dolomite at low temperature. *Proc. Natl. Acad. Sci. U.S.A.* **2013**, *110*, 14540−14545.

(63) Xu, J.; Yan, C.; Zhang, F.; Konishi, H.; Xu, H.; Teng, H. H. Testing the cation-hydration effect on the crystallization of Ca-Mg-CO_3 systems. *Proc. Natl. Acad. Sci. U.S.A.* **2013**, *110*, 17750−17755.

(64) Jiao, D.; King, C.; Grossfield, A.; Darden, T. A.; Ren, P. Simulation of Ca^{2+} and Mg^{2+} solvation using polarizable atomic multipole potential. *J. Phys. Chem. B* **2006**, *110*, 18553−18559.

(65) Tommaso, D. D.; De Leeuw, N. H. Structure and dynamics of the hydrated magnesium ion and of the solvated magnesium carbonates: Insights from first principles simulations. *Phys. Chem. Chem. Phys.* **2010**, *12*, 894−901.

(66) Yang, Y.; Sahai, N.; Romanek, C. S.; Chakraborty, S. A computational study of Mg^{2+} dehydration in aqueous solution in the presence of HS^- and other monovalent anions-Insights to dolomite formation. *Geochim. Cosmochim. Acta* **2012**, *88*, 77−87.

(67) Bock, C. W.; Kaufman, A.; Glusker, J. P. Coordination of water to magnesium cations. *Inorg. Chem.* **1994**, *33*, 419−427.

(68) Kenward, P. A.; Ueshima, M.; Fowle, D. A.; Goldstein, R. H.; Gonzalez, L. A.; Robers, J. A. Ordered low-temperature dolomite mediated by carboxyl-group density of microbial cell walls. *AAPG Bull.* **2013**, *97*, 2113−2125.

(69) Couradeau, E.; Benzerara, K.; Gérard, E.; Moreira, D.; Bernard, S.; Brown, G. E., Jr.; Lopez-Garcfa, P. An early-branching microbialite cyanobacterium forms Intracellular carbonates. *Science* **2012**, *336*, 459−462.

(70) Benzerara, K.; Skouri-Panet, F.; Li, J. H.; Férard, C.; Gugger, M.; Laurent, T.; Couradeau, E.; Ragon, M.; Cosmidis, J.; Menguy, N.; Margaret-Oliver, I.; Tavera, R.; López-García, P.; Moreira, D. Intracellular Ca-carbonate biomineralization is widespread in cyanobacteria. *Proc. Natl. Acad. Sci. U.S.A.* **2014**, *111*, 10933−10938.

(71) Han, Z. Z.; Zhao, Y. Y.; Yan, H. X.; Zhao, H.; Han, M.; Sun, B.; Meng, R. R.; Zhuang, D. X.; Li, D.; Gao, W. J.; Du, S. Y.; Wang, X. A.; Fan, K. X.; Hu, W. Y.; Zhang, M. X. The characterization of intracellular and extracellular biomineralization induced by *Synechocystis sp.* PCC6803 cultured under low Mg/Ca ratios conditions. *Geomicrobiol. J.* **2017**, *34*, 362−373.

(72) Ragon, M.; Benzerara, K.; Moreira, D.; Tavera, R.; Hahn, M. W. 16S rDNA-based analysis reveals cosmopolitan occurrence but limited diversity of two cyanobacterial lineages with contrasted patterns of intracellular carbonate mineralization. *Front. Microbiol.* **2014**, *5*, 331.

(73) Martignier, A.; Pacton, M.; Filella, M.; et al. Intracellular amorphous carbonates uncover a new biomineralization process in eukaryotes. *Geobiology* **2017**, *15*, 240−253.

(74) Yan, H. X.; Owusu, D. C.; Han, Z. Z.; Zhao, H.; Ji, B.; Zhao, Y. Y.; Tucker, M. E.; Zhao, Y. H. Extracellular, surface, and intracellular biomineralization of *Bacillus subtilis* Daniel-1 bacteria. *Geomicrobiol. J.* **2021**, *38*, 698−708.

(75) Li, D.; Zhao, H.; Li, G. J.; Yan, H. X.; Han, Z. Z.; Chi, X. Q.; Meng, L.; Wang, J. H.; Xu, Y. D.; Tucker, M. E. Calcium ion biorecovery from industrial wastewater by *Bacillus amyloliquefaciens* DMS6. *Chemosphere* **2022**, *298*, 134328.

(76) Coronado, M. J.; Vargas, C.; Hofemeister, J.; Ventosa, A.; Nieto, J. Production and biochemical characterization of an @a-amylase from the moderate halophile *Halomonas meridiana. FEMS Microbiol. Lett.* **2000**, *183*, 67−71.

(77) Zhao, Y. Y.; Yan, H. X.; Zhou, J. X.; Tucker, M. E.; Han, M.; Zhao, H.; Mao, G. Z.; Zhao, Y. F.; Han, Z. Z. Minerals bio-precipitation of calcium and magnesium ions through extracellular and intracellular process induced by *Bacillus licheniformis* SRB2. *Minerals* **2019**, *9*, 526.

(78) Pastor, J. M.; Bernal, V.; Salvador, M.; Argandona, M.; Vargas, C.; Csonka, L.; Sevilla, A.; Iborra, J. L.; Nieto, J. J.; Canovas, M. Role of central metabolism in the osmoadaptation of the Halophilic Bacterium *Chromohalobacter salexigens. J. Biol. Chem.* **2013**, *288*, 17769−17781.

(79) Li, X.; Yu, Y. H. Biodiversity and screening of halophilic bacteria with hydrolytic and antimicrobial activities from Yuncheng Salt Lake, China. *Biologia* **2015**, *70*, 151−156.

(80) Rivadeneyra, M. A.; Delgado, R.; Párraga, J.; Ramos-Cormenzana, A.; Delgado, G. Precipitation of minerals by 22 species of moderately halophilic bacteria in artificial marine salts media: Influence of salt concentration. *Folia Microbiol.* **2006**, *51*, 445−453.

(81) Hermans, J.; André, L.; Navez, J.; Philippe, P.; Dubois, P. Relative influences of solution composition and presence of intracrystalline proteins on magnesium incorporation in calcium carbonate minerals: Insight into vital effects. *J. Geophys. Res.* **2011**, *116*, No. G01001.

(82) Walter, L. M.; Morse, J. W. The dissolution kinetics of shallow marine carbonates in seawater: A laboratory study. *Geochim. Cosmochim. Acta* **1985**, *49*, 1503−1513.

(83) Pickett, M. *Dissolution Rates of Biogenic Carbonates in Natural Seawater at Different pCO_2 Conditions: A Laboratory Study*; University of California: San Diego, 2014; pp 1−55.

(84) Ries, J. B.; Ghazaleh, M. N.; Connolly, B.; Westfield, I.; Castillo, K. D. Impacts of seawater saturation state ($\Omega A = 0.4$-4.6) and temperature (10, 25 °C) on the dissolution kinetics of whole-shell biogenic carbonates. *Geochim. Cosmochim. Acta* **2016**, *192*, 318−337.

(85) Plummer, L. N.; Mackenzie, F. T. Predicting mineral solubility from rate data; application to the dissolution of magnesian calcites. *Am. J. Sci.* **1974**, *274*, 61−83.

(86) Blue, C. R.; Giuffre, A.; Mergelsberg, S.; Han, N.; De Yoreo, J.; Dove, P. M. Chemical and physical controls on the transformation of amorphous calcium carbonate into crystalline $CaCO_3$ polymorphs. *Geochim. Cosmochim. Acta* **2017**, *196*, 179−196.

(87) Purgstaller, B.; Dietzel, M.; Baldermann, A.; Mavromatis, V. Control of temperature and aqueous Mg^{2+}/Ca^{2+} ratio on the (trans-)formation of ikaite. *Geochim. Cosmochim. Acta* **2017**, *217*, 128−143.

(88) Swainson, I. P. The structure of monohydrocalcite and the phase composition of the beachrock deposits of Lake Butler and Lake Fellmongery, South. Australia. *Am. Mineral.* **2008**, *93*, 1014−1018.

(89) George, M. G.; Julia, A. B.; Timothy, G. L. Taxonomic Outlines of Prokaryotes. In *Bergey's Manual of Taxonomic*; 2nd ed.; Bacteriology Springer: New York, 2004.

(90) Smith, K. S.; Ferry, J. G. A Plant-Type (β-Class) carbonic anhydrase in the thermophilic methanoarchaeon methanobacterium thermoautotrophicum. *J. Bacteriol.* **1999**, *181*, 6247−6253.

(91) Jagadeesha-Kumar, B. G.; Prabhakara, R.; Pushpa, H. Bio mineralisation of calcium carbonate by different bacterial strains and their application in concrete crack remediation. *Int. J. Adv. Eng. Technol.* **2013**, *6*, 202−213.

(92) Han, Z. Z.; Li, D.; Zhao, H.; Yan, H. X.; Li, P. Y. Precipitation of carbonate minerals induced by the halophilic *Chromohalobacter israelensis* under high salt concentrations: Implications for natural environments. *Minerals* **2017**, *7*, 95.